2009-12

An experimental study of fluid structure interaction of carbon composites under low velocity impact

Owens, Angela C.

Monterey, California. Naval Postgraduate School

NAVAL POSTGRADUATE SCHOOL

MONTEREY, CALIFORNIA

THESIS

AN EXPERIMENTAL STUDY OF FLUID STRUCTURE INTERACTION OF CARBON COMPOSITES UNDER LOW VELOCITY IMPACT

by

Angela C. Owens

December 2009

Thesis Advisor:	Young W. Kwon
Second Reader:	Jarema M. Didoszak

Approved for public release; distribution is unlimited.

THIS PAGE INTENTIONALLY LEFT BLANK

REPORT DOCUMENTATION PAGE			Form Approved OMB No. 0704-0188
Public reporting burden for this collection of information is estimated to average 1 hour per response, including the time for reviewing instruction, searching existing data sources, gathering and maintaining the data needed, and completing and reviewing the collection of information. Send comments regarding this burden estimate or any other aspect of this collection of information, including suggestions for reducing this burden, to Washington headquarters Services, Directorate for Information Operations and Reports, 1215 Jefferson Davis Highway, Suite 1204, Arlington, VA 22202-4302, and to the Office of Management and Budget, Paperwork Reduction Project (0704-0188) Washington DC 20503.			
1. AGENCY USE ONLY ***(Leave blank)***	**2. REPORT DATE** December 2009	**3. REPORT TYPE AND DATES COVERED** Master's Thesis	
4. TITLE AND SUBTITLE Experimental Study of Fluid Structure Interaction of Carbon Composites under Low Velocity Impact		**5. FUNDING NUMBERS**	
6. AUTHOR(S) Angela C. Owens			
7. PERFORMING ORGANIZATION NAME(S) AND ADDRESS(ES) Naval Postgraduate School Monterey, CA 93943-5000		**8. PERFORMING ORGANIZATION REPORT NUMBER**	
9. SPONSORING /MONITORING AGENCY NAME(S) AND ADDRESS(ES) N/A		**10. SPONSORING/MONITORING AGENCY REPORT NUMBER**	
11. SUPPLEMENTARY NOTES The views expressed in this thesis are those of the author and do not reflect the official policy or position of the Department of Defense or the U.S. Government.			
12a. DISTRIBUTION / AVAILABILITY STATEMENT Approved for public release; distribution is unlimited.		**12b. DISTRIBUTION CODE**	

13. ABSTRACT (maximum 200 words)

The effect of fluid force on the natural frequencies and damping ratios of vibrating structures in contact with fluid is known as the Fluid Structure Interaction (FSI) problem. It can be interpreted as an added mass to the vibrating structure in the analysis of the dynamic response. Because the density of water is much greater than air, the added mass effect becomes even more critical in understanding the dynamic response of composites in water surroundings.

In this study, experimental testing was carried out to investigate FSI of composite laminates immersed in fluid and subjected to low-velocity impact. Square composite laminates of carbon fiber weave and vinyl ester resin of size 305 mm and 2.38 mm nominal thickness were subjected to low velocity impact loading, using a specially developed vertical drop-weight testing machine. The composite samples were fitted with gages to provide real-time information on strain levels generated during impact. Impact tests were performed on four side clamped laminates in air-backed, water-backed, and dry surroundings, and at various impact energies for investigation. The findings of this study will provide a better understanding for the use of composite materials in underwater structural applications where impact loading is expected.

14. SUBJECT TERMS Composite, Carbon, Low Velocity Impact, Fluid Structure Interaction			**15. NUMBER OF PAGES** 66
			16. PRICE CODE
17. SECURITY CLASSIFICATION OF REPORT Unclassified	**18. SECURITY CLASSIFICATION OF THIS PAGE** Unclassified	**19. SECURITY CLASSIFICATION OF ABSTRACT** Unclassified	**20. LIMITATION OF ABSTRACT** UU

NSN 7540-01-280-5500 Standard Form 298 (Rev. 2-89)
Prescribed by ANSI Std. 239-18

THIS PAGE INTENTIONALLY LEFT BLANK

Approved for public release; distribution is unlimited.

AN EXPERIMENTAL STUDY OF FLUID STRUCTURE INTERACTION OF CARBON COMPOSITES UNDER LOW VELOCITY IMPACT

Angela C. Owens
Lieutenant, United States Navy
B.S., Old Dominion University, 2002

Submitted in partial fulfillment of the
requirements for the degree of

MASTER OF SCIENCE IN MECHANICAL ENGINEERING

from the

NAVAL POSTGRADUATE SCHOOL
December 2009

Author: Angela C. Owens

Approved by: Young W. Kwon
Thesis Advisor

Jarema M. Didoszak
Second Reader

Knox T. Millsaps
Chairman, Department of Mechanical and Astronautical Engineering

THIS PAGE INTENTIONALLY LEFT BLANK

ABSTRACT

The effect of fluid force on the natural frequencies and damping ratios of vibrating structures in contact with fluid is known as the Fluid Structure Interaction (FSI) problem. It can be interpreted as an added mass to the vibrating structure in the analysis of the dynamic response. Because the density of water is much greater than air, the added mass effect becomes even more critical in understanding the dynamic response of composites in water surroundings.

In this study, experimental testing was carried out to investigate FSI of composite laminates immersed in fluid and subjected to low-velocity impact. Square composite laminates of carbon fiber weave and vinyl ester resin of size 305 mm and 2.38 mm nominal thickness were subjected to low velocity impact loading, using a specially developed vertical drop-weight testing machine. The composite samples were fitted with gages to provide real-time information on strain levels generated during impact. Impact tests were performed on four side clamped laminates in air-backed, water-backed, and dry surroundings, and at various impact energies for investigation. The findings of this study will provide a better understanding for the use of composite materials in underwater structural applications where impact loading is expected.

THIS PAGE INTENTIONALLY LEFT BLANK

TABLE OF CONTENTS

THIS PAGE INTENTIONALLY LEFT BLANK

LIST OF FIGURES

LIST OF TABLES

THIS PAGE INTENTIONALLY LEFT BLANK

ACKNOWLEDGMENTS

First and foremost, I would like to thank Dr. Young Kwon for his mentorship during the course of this research and throughout my graduate studies. I would also like to thank Tom Christian for design of the analyzer and his guidance during the testing phase of this research.

Thank you to Advanced Hull Materials & Structures Technology Division of Naval Surface Warfare Center Carderock who provided materials, and to the Office of Naval Research for financial support.

I. INTRODUCTION

A. BACKGROUND

The growing use of composites in ship masts, superstructures, deck grates, piping, ducting, rudders, propellers, stacks, and various submarine structures requires extensive modeling and testing to help designers, builders and operators better understand composite response [1]. These materials are subjected to a wide spectrum of loadings during manufacturing and service life. Dynamic loadings, in particular, impact type events, represent a serious design concern for use of composites because composite structures are more susceptible to impact damage than similar metallic structures that are ductile in nature and can absorb large amounts of energy without failure [2]. Also, the damage in composites from impact can go undetected, even when the mechanical properties may be drastically reduced from the impact. For these reasons, numerous experimental and analytical studies have been conducted to study the dynamic response of composites subjected to transient dynamic loading. In an article completed in 1994 on the recent advances on impact on laminated composites, Serge Abrate reviewed over 300 articles and provided a comprehensive view of the state of knowledge in the area [3]. According to Abrate, most of the current research effort is focused on low velocity impact damage, in particular, the damage predictions and the evaluation and prediction of residual properties of damaged laminates. All of the research completed has been on composites under low velocity impact in dry surroundings to support development of composites in aircraft structures.

Assemblages of layers of composite fibers, known as a laminate, can be tailored to provide a wide range of engineering properties, including in plane stiffness, bending stiffness, strength, and coefficients of thermal expansion [4]. Each individual layer consists of a high-modulus, high-strength fiber in a ceramic, metallic, or polymeric material. However, composites are inherently weak in the transverse direction—the thickness— because there are no fibers present in that direction [5]. Current types of fibers in use include carbon, glass, silicon carbide, and Kevlar. Carbon is widely used in structural applications because it has the highest strength and stiffness values; however, it

is also the most brittle, with a strain to failure of 0.5% to 2.4% [6]. Composite fibers are manufactured in a unidirectional or woven layout.

Recent advancements have determined that woven fabric composites, due to the interlacing of fiber rows in two directions, offer better resistance as compared to unidirectional composites [7]. Matrix materials commonly used are epoxies, aluminum, titanium, and alumina, or a hybrid matrix of mixed materials. In laminates, several assumptions are made: a) that there is perfect bonding between the layers, b) that each layer can be represented as an homogeneous material with known effective properties that may be isotropic, orthotropic, or transversely isotropic, c) that each layer is in a state of plane stress, and d) that the laminate deforms according to the Kirchhoff assumptions for bending and stretching of thin plates [8].

Generally, impacts are characterized as low, high, or hyper velocity. Researchers tend to disagree on how to categorize events into the impact categories, but generally, it is based on the type of damage induced. In the Abrate review, low velocity impact is defined as impact at speeds of less than $100\,ms^{-1}$. Low velocity impacts are of great concern because the effects are generally undetected, since the level of impact that causes visible damage is much higher than the level at which substantial loss of residual properties occur [9]. Low velocity impacts are expected to occur during manufacturing and during service life.

As important as the ongoing research of response of composites to dynamic loading, a great amount of analytical and experimental studies have been conducted on the effect of fluid force on the natural frequencies, damping ratios, and mode shapes of vibrating structures in contact with fluid, known as the Fluid Structure Interaction (FSI) problem. FSI investigations have supported many problems in submarine signaling and ship structure vibrations. Through these studies, many numerical and analytical methods have been development in order to predict the added mass and the resulting changes in natural frequency of a structure in contact with fluid. It has been determined and widely proven that the effect of fluid decreases the natural frequency of a structure due to the increase in total kinetic energy of the vibrating structure and fluid from the addition of kinetic energy of the fluid. This effect can be interpreted as an added mass to the

vibrating structure in the analysis of the dynamic response. Essentially, as the structure vibrates, its mass is increased by the mass of the vibrating fluid in contact, consequently decreasing its natural frequency. Studies of fluid structure interaction and the added mass effect, also known as virtual mass effect, hydrodynamic mass, and hydroelastic vibration of structures, started in 1920 with Lamb [10], who calculated the first bending mode of a submerged circular plate. In response to a problem of submarine signaling, Lamb investigated the vibrations of a thin elastic circular plate in contact with water. In his investigation, he discovered that the natural frequencies for structures in contact with fluid are lower than the frequencies in air, based on the assumption that the modes shapes are virtually the same in water as in a vacuum. The resonant frequency was determined using Rayleigh's method. Powell and Roberts [11] experimentally verified Lam's theoretical results. Lindholm et al. [12], Volcy et al. [13], and Fu and Price [14] did extensive experimental studies on the response of cantilever plates under various orientations, boundary conditions, geometrical shapes and levels of submergence. The above studies were mainly focused on the fundamental mode of a circular plate. Kwak and Kim [15] investigated the problem of axisymmetric vibration of circular plates. They, by employing the Hankel transform, solved the mixed boundary problem and calculated the nondimensionalized added virtual mass incremental (NAVMI) factors for higher modes of clamped, simply supported, and free plates. The NAVMI factor is the ratio of kinetic energy of water and the kinetic energy of the plate based on the assumption that the mode shape does not change under the influence of water. They also determined that for plates in contact with water on two sides, the NAVMI factor is twice the value for a plate in contact on only one side. Kwak [16] calculated the added virtual mass of rectangular plates with simply supported and clamped boundary conditions vibrating in contact with water. The Green function was used to solve the boundary value problem of the water domain. This method was combined with the Rayleigh-Ritz method. Haddara and Cao [17] presented analytical and experimental studies of the dynamic response of submerged rectangular plates. An approximate expression to calculate the modal added mass for flat rectangular plates was developed and compared to experimental results.

B. OBJECTIVES

The work presented herein is focused on the investigation of the added mass effect on the dynamic response of clamped composite square plates submerged in water. Because the density of composites is nearly equivalent to that of the density of water, the added mass effect of the water becomes even more critical to understand the dynamic response of composites in water surroundings. The purpose of this study is to perform the forced vibration analysis of carbon woven fiber/vinyl ester resin composite laminates submerged in water and subjected to low velocity impact. The impact testing was conducted with a specifically developed vertical drop weight testing apparatus, and the composite samples were fitted with gages to provide real-time information on strain levels generated during impact. The transient response of the sample included load and strain as a function of time. Samples were constructed using the Vacuum Assisted Resin Transfer Molding (VARTM) technique. Many tests were performed to verify repeatability. Phases of research included testing the samples in various environmental surroundings: dry surrounding, top wet/air-backed, and top wet/water-backed. The dry phase was completed as the baseline for comparison of the other phases of research in order to identify the change in response of the composite from the fluid surrounding. Finally, a comparison of various impact velocities was studied. The findings of this study will provide a better understanding for use of composite materials in underwater structural applications where impact loading is expected.

II. EXPERIMENTAL TECHNIQUE

A. COMPOSITE FABRICATION

Five carbon fiber laminate samples were constructed during the course of this research. Each sample was fabricated from TORAY T700CF carbon fiber bidirectional weave and DERAKANE 510-A vinyl-ester matrix resin. These materials were selected by the Naval Surface Warfare Center Carderock Advanced Hull Materials & Structures Technology Division because they are used for naval vessels. Each plate was fabricated through the VARTM process, which consists of pulling resin through layers of carbon fibers using a vacuum. Hardening chemicals were added to the resin base to achieve a nominal 60 minute curing time to avoid air bubble formation in the samples. The samples all had dimensions of 457 x457 mm, thickness of 2.38 mm, and a density of 1.6 g/cm^3.

1. Sample Preparation

The plates fabricated for this study were square 8 ply laminates at 457 mm at 2.38 mm thick. The layers of the laminate were stacked aligned at [0/90/0/90].

2. Resin Preparation

The DERAKANE resin was mixed with three hardeners: Methyl Ethyl Ketone Peroxide (MEKP), Cobalt Napthenate (CoNAP), and N, N- Dimethylaniline (DMA) to achieve a nominal 60 minute curing time. The hardeners used are to achieve proper gel time and do not affect composite strength [5]. All resin components were mixed based on a percent weight for a nominal cure time per manufacturer's directions at a temperature of less than 70ºF. The DERAKANE 510-A was measured by volume, and the MEKP, CoNAP, and DMA were measured by weight. The measurements are summarized in Table 1.

Table 1. Summary of hardener measurements for resin preparation

Component	Amount
DERAKANE 510-A	1 Liter
Methyl Ethyl Ketone Peroxide (MEKP)	15.866 g
Cobalt Napthenate (CoNAP)	2.533 g
N, N- Dimethylaniline (DMA)	0.633 g

3. VARTM setup and procedure

Setup and procedure concerning the Vacuum Assisted Resin Transfer Molding (VARTM) technique for fabricating composite materials was provided by Naval Surface Warfare Center Carderock Division (NSWCCD). The VARTM apparatus consists of a glass surface, resin reservoir, vacuum pump, gage board, and resin trap as shown in Figures 1 and 2.

Figure 1. Fabrication of samples by VARTM process

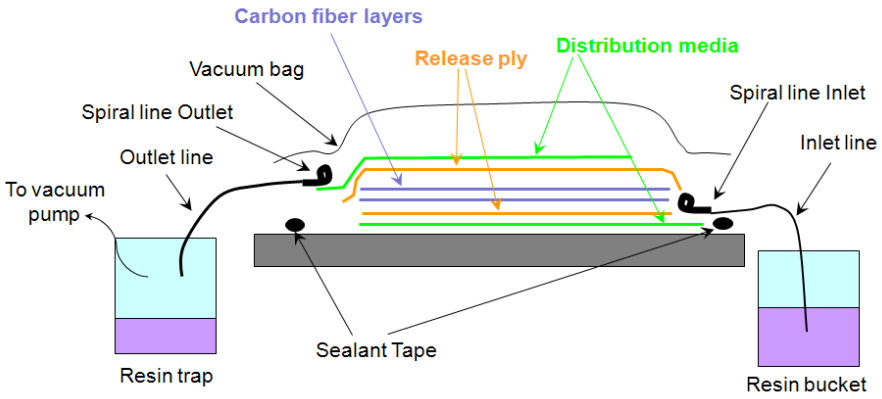

Figure 2. VARTM setup description

The glass working surface is made of a sheet of 12 mm thick tempered glass for hardness, durability, and thermodynamic properties, and to promote the proper seal for the vacuum bag. The pump provides the vacuum necessary to draw the resin from the resin reservoir through the composite sample, and ensures a vacuum seal to prevent air from entering the composite sample. The gage board measures and regulates the vacuum pressure in the sample. The purpose of the resin trap is to allow air from the sample to pass freely through the gage board to the vacuum pump while simultaneously preventing the resin from contaminating these sensitive components by providing collection reservoir. After a satisfactory vacuum was established and all air leaks in the vacuum bag assembly were eliminated, inlet tubing is inserted into the resin reservoir, allowing the resin to flow through the composite sample. A detailed description of the VARTM procedure is provided in Table 2.

Table 2. Detailed VARTM procedure

Step 1	Place a layer of peel ply on glass working surface.
Step 2	Place a sheet of distribution media on top of peel ply.
Step 3	Place a layer of release ply on top of distribution media
Step 4	Cut desired amount of carbon fiber fabric layers to desired size and stack on top of release ply.
Step 5	Place a second layer of release ply on top of carbon fiber fabric.
Step 6	Place a sheet of distribution media on top of release ply.
Step 7	Set up resin inlet tubing from the reservoir and outlet tubing through the resin trap.
Step 8	Attach plastic sheet using putty/tape on top of layers to act as a vacuum bag.
Step 9	Perform vacuum check to reach 26 inches Hg.
Step 10	Mix resin and hardeners under a fume hood and wait approximately 10 minutes for air bubbles to stop forming.
Step 11	Insert inlet tube into resin reservoir and allow resin to flow into carbon fiber layers. (See Figure 3)
Step 12	Maintain vacuum for 60 minutes.
Step 13	Allow sample to sit at least 24 hours before removing sample from VARTM set up.

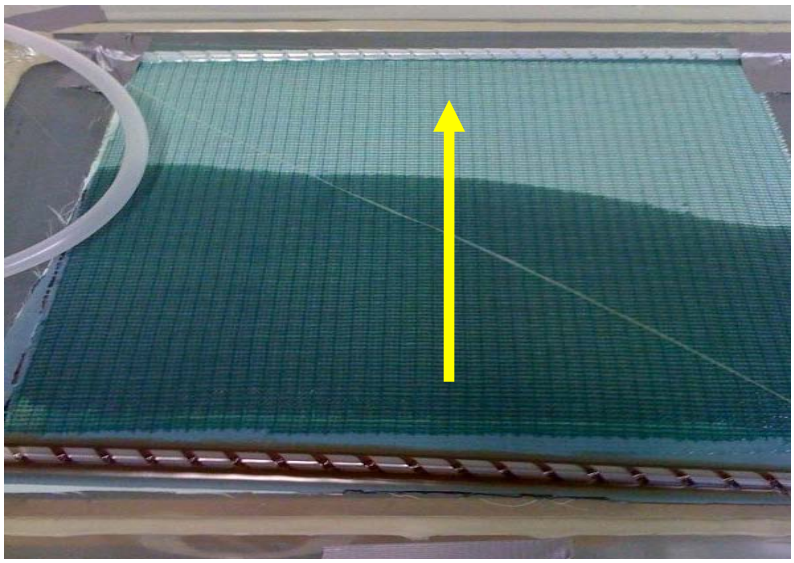

Figure 3. Resin flow through carbon fiber layers

B. APPARATUS

Impact tests were conducted using a specially designed drop weight instrumented testing system that consisted of a drop weight impactor, load transducer, strain gages, high speed data analyzer, and an air box, as shown in Figure 4. The samples were supported between two aluminum plates with a square 305 mm cutout in the center. The plates were then clamped to the impactor frame using c-clamps of dimensions 76 mm jaw x 60 mm throat to facilitate clamped boundary conditions, as shown in Figure 5. Transient response of the sample included load and strain as a function of time.

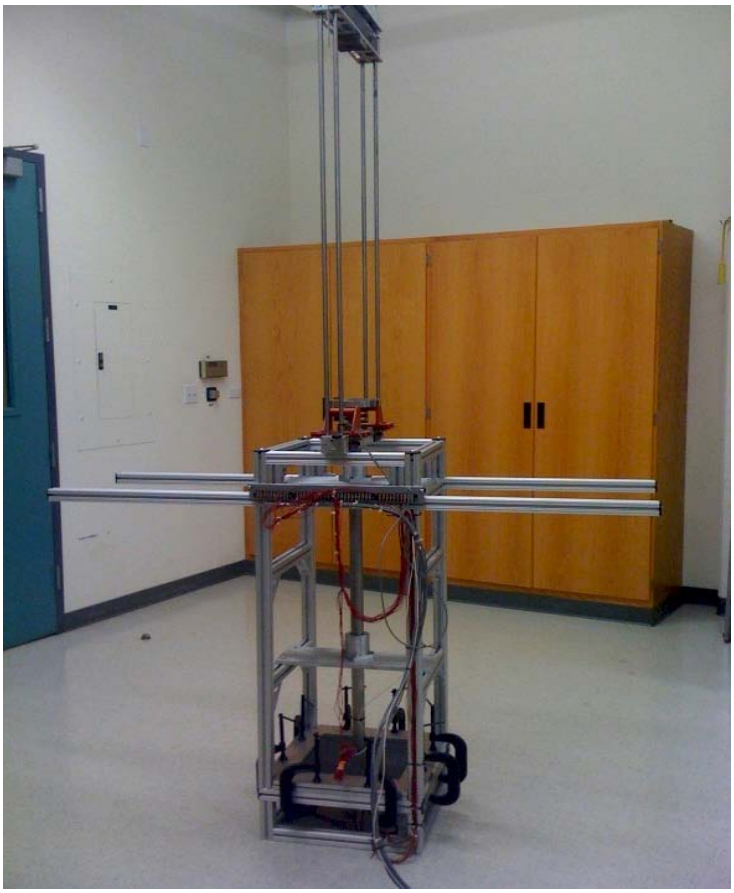

Figure 4. Drop weight instrumented testing system

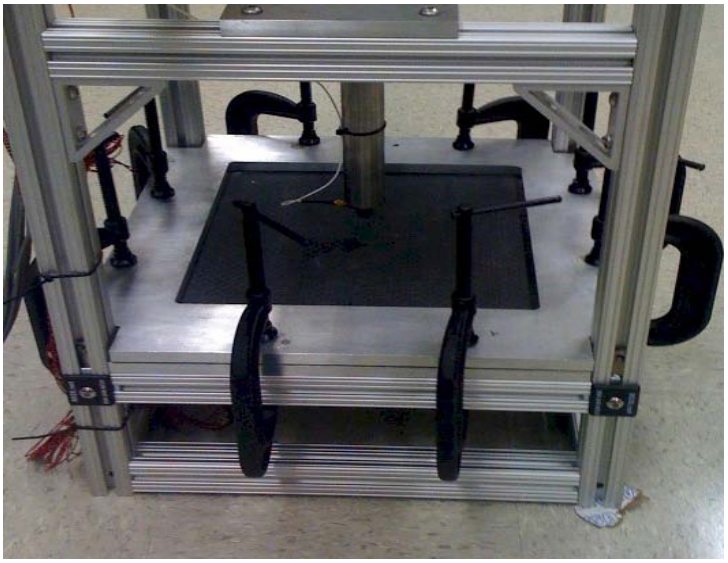

Figure 5. Clamped boundaries of composite sample

1. Drop Weight Impactor

The drop weight impactor consisted of a drop weight and an impact rod. The drop weight was supported by four steel guide rods, and the impact rod was supported by an aluminum frame base. The dimensions of the guide rods were 121.9 cm high with 0.635 cm diameter, and the dimensions of the base frame were 1168 mm high x 457 mm wide x 457 mm deep. The aluminum framing pieces and fasteners were manufactured by 8020, Inc. and assembled at Naval Postgraduate School for this research. The falling weight was guided by four small linear bearings. The impact rod was guided with two plain bushing aluminum linear bearings of 1.5 inch diameter enclosed in a casing for support, as shown in Figure 7. A spring was used to reduce the number of multiple impacts per drop (Figure 8). A trigger at the base of the falling weight was used to initiate data collection. The drop weight was kept constant at 12 kg. The impact rod was made of steel and weighed 12 kg. Impact velocity was varied by changing the drop height, which will be addressed in detail in a later section. The maximum height was 1.07 m, which can produce approximately 4.6 m/s initial velocity upon impact. The impact was at the center of the composite sample.

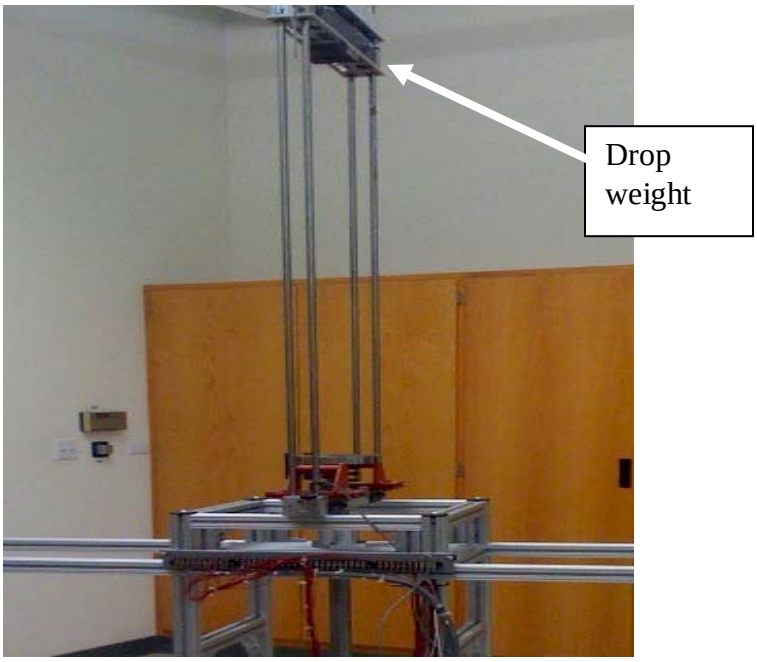

Figure 6. Drop weight and steel guide rods

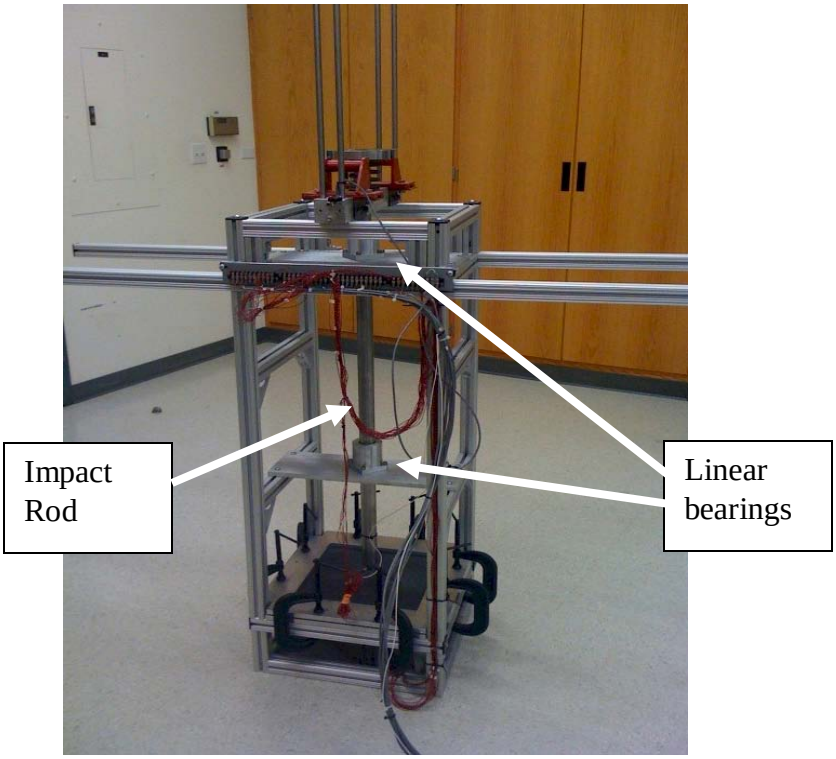

Figure 7. Drop weight impactor base frame

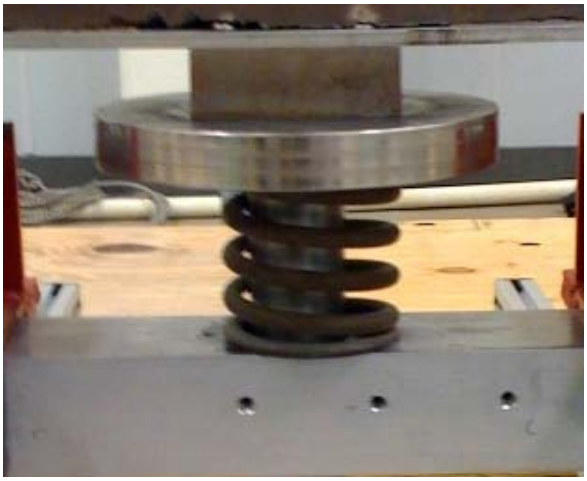

Figure 8. Spring for impact rod

2. Load Transducer

The load cell was an ICP® force sensor manufactured by PCB Piezotronics, Inc., which converts force into a measurable electrical output. The load transducer was mounted on the end of the impactor rod, as shown in Figure 9. The gage had a diameter of 16mm. For wet testing the gage and cable connection were coated with M coat A bond.

Figure 9. Mounted load transducer with sealant

3. Strain Gages

The strain gages were large three-element 45° single-plane rosettes, model CEA-00-250UR-350, by Vishay Micro-Measurements, as illustrated in Figure 10. The advantage of the rectangular rosette is that it allows for the measurements of the extensional strains ε_x and ε_y, as well as the shear strains γ_{xy} simultaneously.

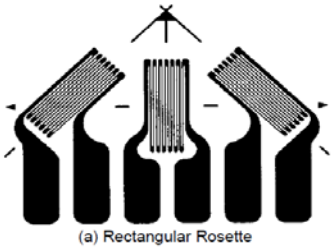

Figure 10. Rectangular rosette strain gage

Each gage consists of a fine metal grid that is stretched or shortened when the sample is strained at the location point of the gage. This change in resistance is then converted into a measurement of strain. The conversions for calculating the strains from the three rosette strain measurements were derived from the strain transformation equations [18]. Given the measurement of three independent strains from the three-gage rosette with 45^o between two neighboring gages, the state of strain at the gage location with respect to any particular x-y axis system using the rosette readings and their axis orientation can be calculated. In solving for the strains in the designated x-y system, as illustrated in Figure 11, the strain transformation equations become

$$\varepsilon_A = \frac{1}{2}(\varepsilon_x + \varepsilon_y) + \frac{1}{2}(\varepsilon_x - \varepsilon_y)\cos(2*0°) + \frac{1}{2}\gamma_{xy}\sin(2*\phi°)$$

$$\varepsilon_B = \frac{1}{2}(\varepsilon_x + \varepsilon_y) + \frac{1}{2}(\varepsilon_x - \varepsilon_y)\cos(2*45°) + \frac{1}{2}\gamma_{xy}\sin(2*\phi°)$$

$$\varepsilon_C = \frac{1}{2}(\varepsilon_x + \varepsilon_y) + \frac{1}{2}(\varepsilon_x - \varepsilon_y)\cos(2*90°) + \frac{1}{2}\gamma_{xy}\sin(2*\phi°)$$

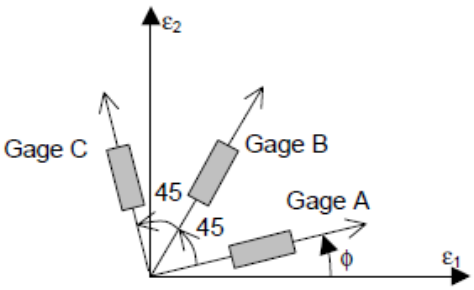

Figure 11. Rectangular rosette gage orientation

By assuming the x-y axis to be aligned with the rosette axis, the strain transformation equations become:

$$\varepsilon_x = \varepsilon_A$$
$$\varepsilon_y = \varepsilon_C$$
$$\gamma_{xy} = 2 * \varepsilon_B - \varepsilon_A - \varepsilon_C$$

This defines the strain state at each location of the rosettes with respect to the designated x-y axis system.

There were four rosette strain gages bonded to each composite sample. The gages were bonded to the underside of the laminate samples, opposite side of impact, using M coat A bond and sealed for waterproofing, as shown in Figure 12.

Figure 12. Rectangular rosette gage bonding

Figure 13 illustrates the orientation and location. Gage 1 was located directly at center on the underside of the sample opposite the impact. Gages 3 and 4 were placed along a diagonal direction of the plate while gage 2 was put on the vertical symmetric line of the plate.

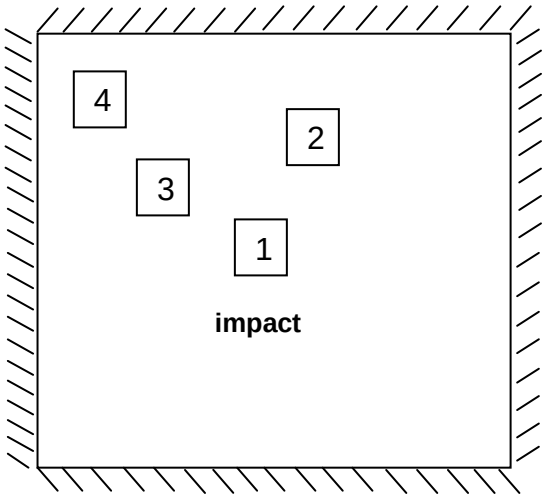

Figure 13. Gage locations on composite sample

4. Data Analyzer

Data acquisition was carried out using a specifically developed acquisition system (Figure 14) that consisted of a Pentium™ 4, 2.4 GHz, 512-MB RAM system, National Instruments™ simultaneous sampling multifunction DAQ, and five Vishay™ 2120 multi-channel strain signal conditioners. The system had a 16 bit analog-to-digital conversion resolution and was capable of reading a total of 16 channels at a throughput rate of up to 250 kS/s per channel, which was appropriate for the rate of testing used in this study. The data-acquisition process was controlled using the NI-DAQmx driver software and LabVIEW™ interactive data-logging software that was specifically formatted at the Naval Postgraduate School for this research. A trigger located at the top of the impact rod was used to initiate data acquisition. Strain readings from five signal conditioners were multiplexed in order to accommodate all strain gages within the available number of channels. Errors due to instrumentation noise did not seem to cause problems in the data, so no filtering was used.

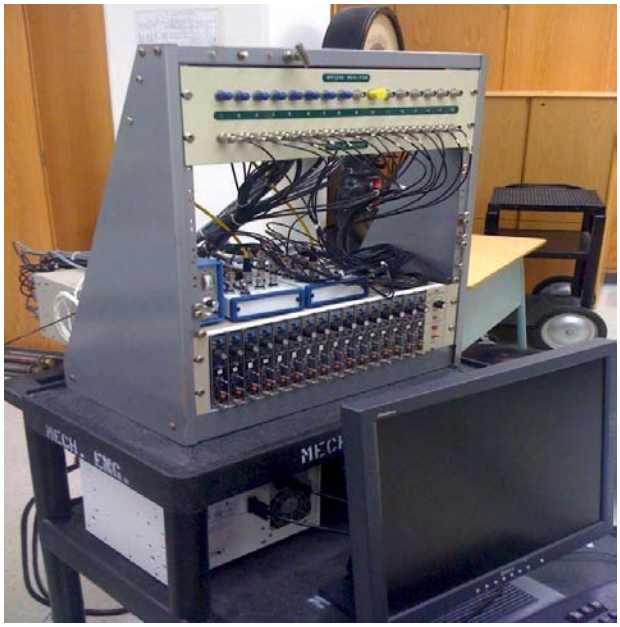

Figure 14. Data acquisition system

5. Air Box

A box was specifically constructed to facilitate phase II testing modeling top wet/bottom dry surroundings, as shown in Figure 15. The box was made of 12.7 mm thick plexi-glass with dimensions 330 mm wide x 330 mm long x 127 mm deep. The box was secured to the bottom aluminum support plate for the composite sample using 8 c-clamps of dimensions 76 mm jaw x 60 mm throat, and sealed with putty tape to prevent water leakage. The box completely covered the sample so that none of the sample was exposed to water. A 19 mm diameter hole was cut out from the side to feed the wiring from the strain gages to the data analyzer, which was filled with putty to prevent water leakage during phase II testing.

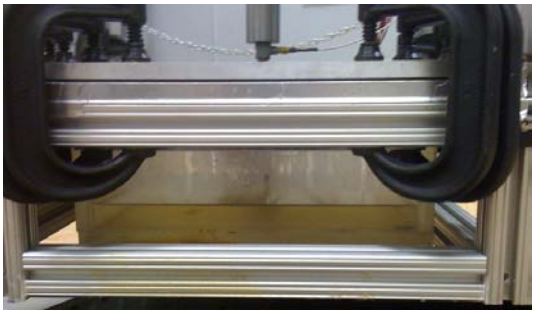

Figure 15. Air box

6. Water Tank

The water tank used for modeling underwater surroundings in phase II and III testing was 2.75 m wide x 2.75 m long x 2.75 m deep. An anechoic tank was used to minimize the influence of the dynamic behavior of the coupled system. The tank was filled with tap water. A standing platform was constructed across the top of the tank made with aluminum I-beams and plywood, leaving a 0.635 m x 0.914 m square opening for the drop weight impactor, as shown in Figure 16.

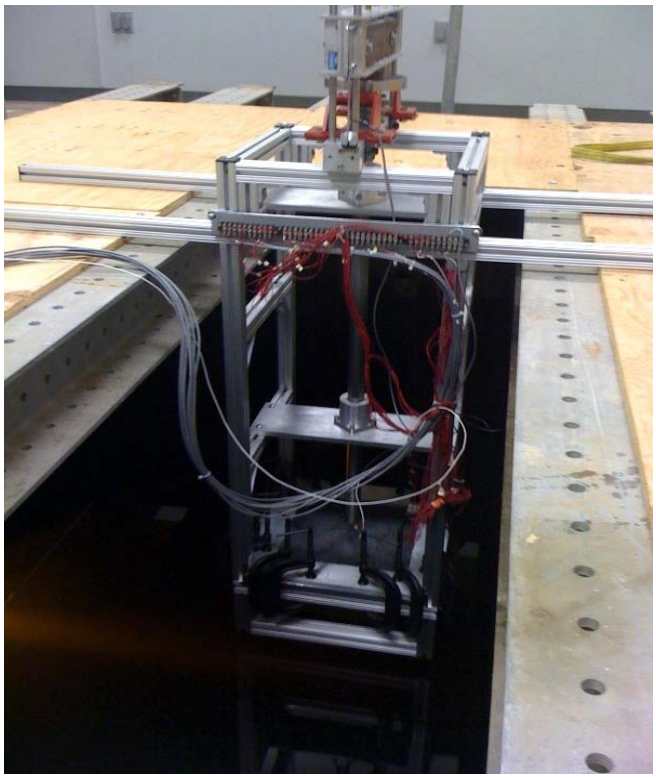

Figure 16. Water tank with drop weight impactor

THIS PAGE INTENTIONALLY LEFT BLANK

III. PHASES OF TESTING

A. PROCEDURE OVERVIEW

There were four phases of testing completed during this research that varied in the simulations of environmental surroundings. Each composite sample was tested in each phase. The first sample was completed to test the strain gage bonding material under impact and in water, to test the force gage under impact and the sealant in water, to test the data acquisition system integration, and to test the trigger for data collection. One of the challenges was finding the right bonding material to get a good bond between the strain gages and the composite. The successful materials and apparatus composition were listed in the experimental technique section.

B. PHASE I-DRY SURROUNDINGS TESTING

Phase I was completed as the baseline for comparison of the other phases of research in order to identify the change in response of the composite from the fluid surrounding. For this testing, the drop weight impactor was suspended in the tank but the water was lowered well below the impactor frame for testing.

C. PHASE II-WET TOP/AIR-BACKED SURROUNDING TESTING

In phase II testing, the tank was filled >15 cm, 50% of the plate length, above the end of the impact rod in order to minimize the disturbance of fluid level on frequency [16]. The drop weight impactor was suspended in the tank, and the air box was sealed to maintain an air-backed environment below the composite.

D. PHASE III-WET TWO SIDE SURROUNDINGS TESTING

In phase III testing, the tank was filled >15 cm, 50% of the plate length, above the end of the impact rod in order to minimize the disturbance of fluid level on frequency [16]. The drop weight impactor was suspended in the tank, and the putty in the hole of the air box used for the strain gage wiring was removed to allow water to fill the air box for a wet environment below the composite.

E. PHASE IV-IMPACT VELOCITY VARIANT TESTING

The effect of impact velocity was investigated in phase IV. It is expected that decreasing the impact velocity decreases the magnitude of impact force and strain; therefore, investigations are focused on the influence of FSI by various impact velocities. Velocity was varied by varying the height the free weight was dropped. There were three heights used, 1.07 m, 0.76 m, and 0.46 m, which correspond to velocities of 4.6 m/sec, 3.9 m/sec, and 3 m/sec. Each varied velocity was tested in each environmental surrounding. Many tests were performed to verify repeatability.

IV. RESULTS AND DISCUSSION

A. OVERVIEW

All composite samples were tested in each phase. Any potential change of composite material properties associated with moisture absorption from water is not considered, in order to make a fair comparison between dry and wet structures.

Each drop test generated 1,000 sample values of each arm of each strain rosette, resulting in a sampling rate of 10,000 per sec. The load transducer produced voltages that were converted to Newton force using the following conversion, where 5.232 *mv*/Lbf is the force gage conversion factor:

$$F(N) = ((samplevalue * 1000) / 5.232) * 4.448$$

The rectangular rosette strain gages were connected into a Wheatstone bridge circuit. The output voltage from the bridge:

$$v = \frac{BV * GF * \varepsilon * 20}{4}$$

Where BV is the bridge excitation voltage at 9.66 and GF is the gain factor at 2. In solving for strain:

$$\varepsilon = \frac{4 * v}{(20 * 9.66 * 2)}$$

The data analysis program converted the data directly to Microsoft® Excel. Force gage data offsets due to AC coupling, which can cause a charge remaining in the capacitor causing a non-zero baseline of the settling value, were adjusted to a zero baseline. Strain gage data offsets as a result of the differences in volts of the output nodes of the Wheatstone bridge were also adjusted to a zero baseline.

Many tests of each phase were completed in order to confirm repeatability of testing data. A representative sample of each phase is illustrated and discussed in each of the following sections. Experimental natural frequency and damping ratio of the system were calculated and compared to theoretical approximations.

B. PHASE I, II, III COMPARISON

Phase I, the dry surroundings phase, was completed as the baseline for comparison of the other phases of research in order to identify the change in response of the composite from the fluid surrounding. In phase II testing, the surroundings of the composite sample were top wet and air-backed, designated wet-t. In phase III testing, the surroundings of the composite sample were top wet and water-backed, designated wet-2.

1. Experimental Results Response Plots

Figures 17–23 illustrate a representative sample of the dynamic response of the composite plate under both wet surroundings compared to the baseline representative sample.

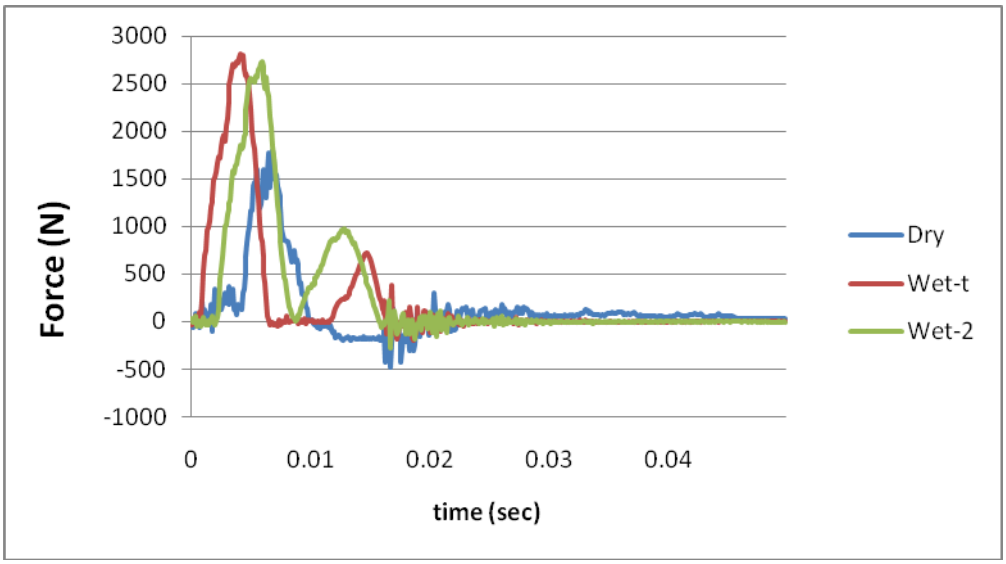

Figure 17. Representative transient force response

As shown in Figure 17, the measured impact force for the air-backed and water-backed wet cases were 55% and 50% greater than the dry case, respectively. The higher magnitude in both wet cases is the effect of the added mass. A series of finite element analyses were conducted to verify that the higher magnitude was indeed due to added mass. In the numerical study, it was determined that because the density of water is of the same order as the composite, the mass is essentially doubled, which causes the plate

to respond slower, which causes the contact force between the plate and the load gage to be larger, which is represented as a higher impact force.

The peak impact force occurs earliest for the air-backed wet impact, followed by the water-backed case, and latest for the dry impact. The dry impact shows an early small bump of oscillation and a delay in peak response that does not occur in either wet impacts. This seems to be part of the added mass effect because it follows the proportions of magnitude of added mass, where the air-backed case has the highest added mass, then the water-backed case, and then the dry, and also because it occurred in later tests with varied velocities.

The second peak force for both wet cases is a second impact that was not prevented by the spring. The air-backed case displayed a delay between impacts, whereas in the water-backed case the secondary peak immediately followed the initial peak.

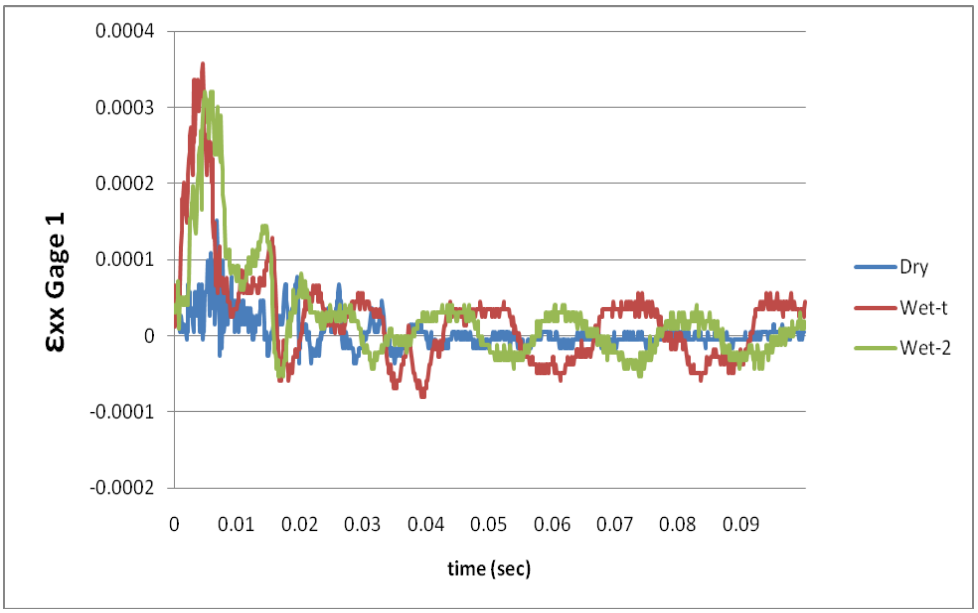

Figure 18. Representative ε_{xx} gage 1 response

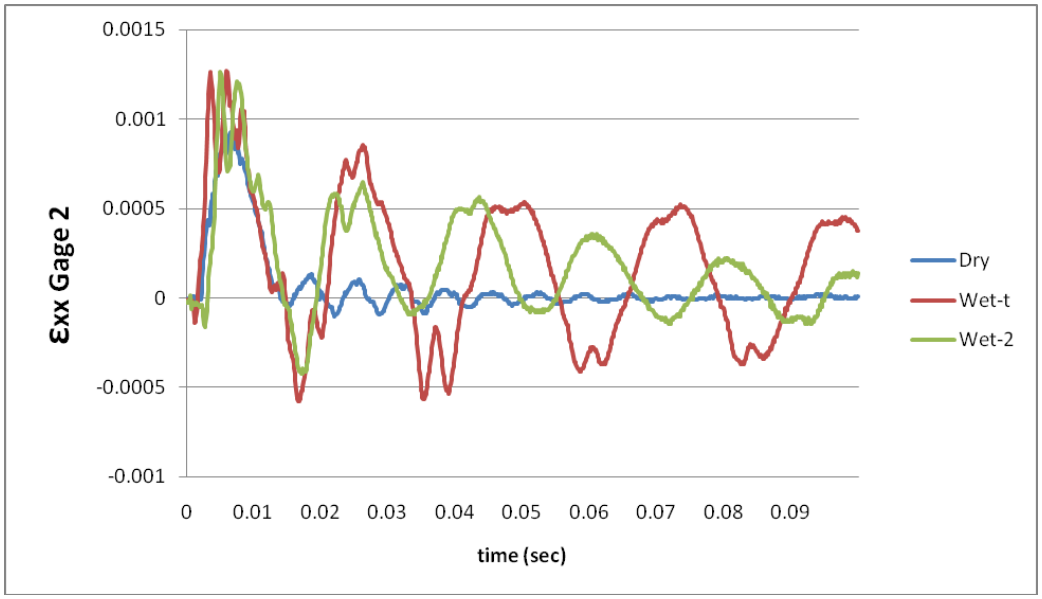

Figure 19. Representative ε_{xx} gage 2 response

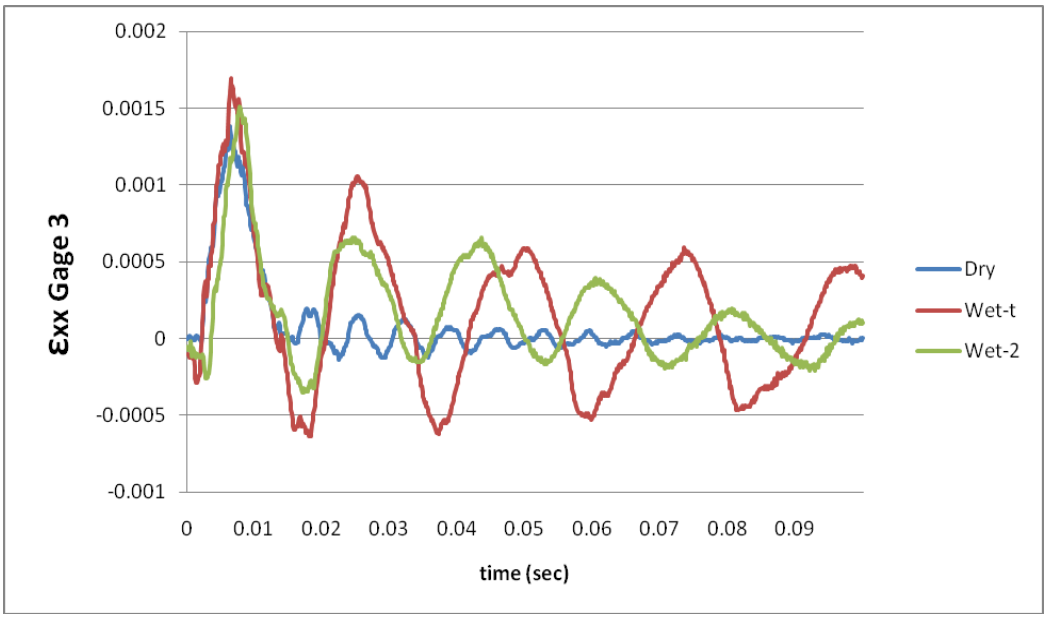

Figure 20. Representative ε_{xx} gage 3 response

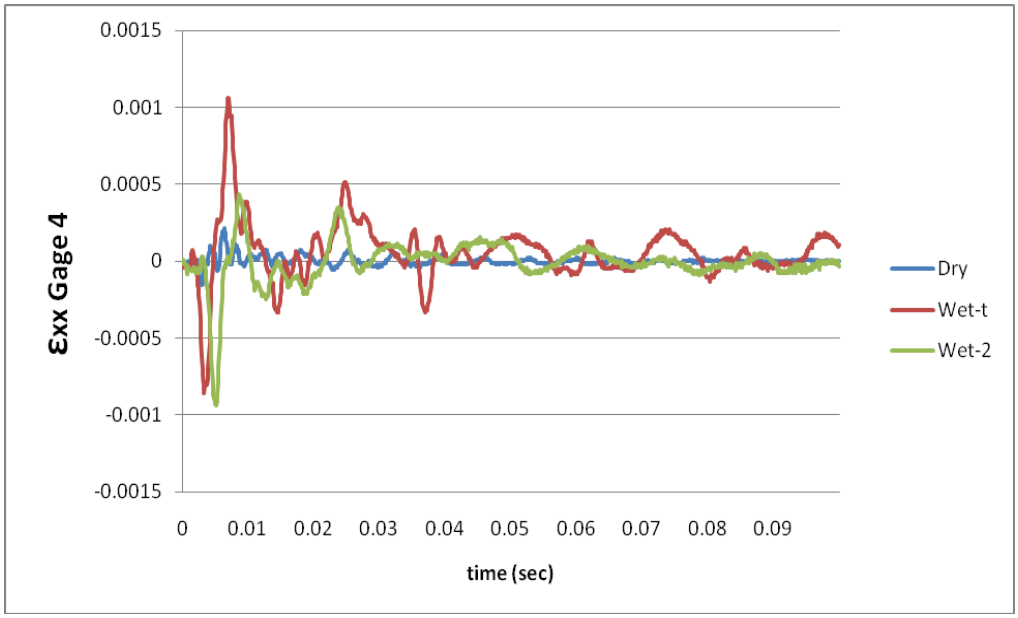

Figure 21. Representative ε_{xx} gage 4 response

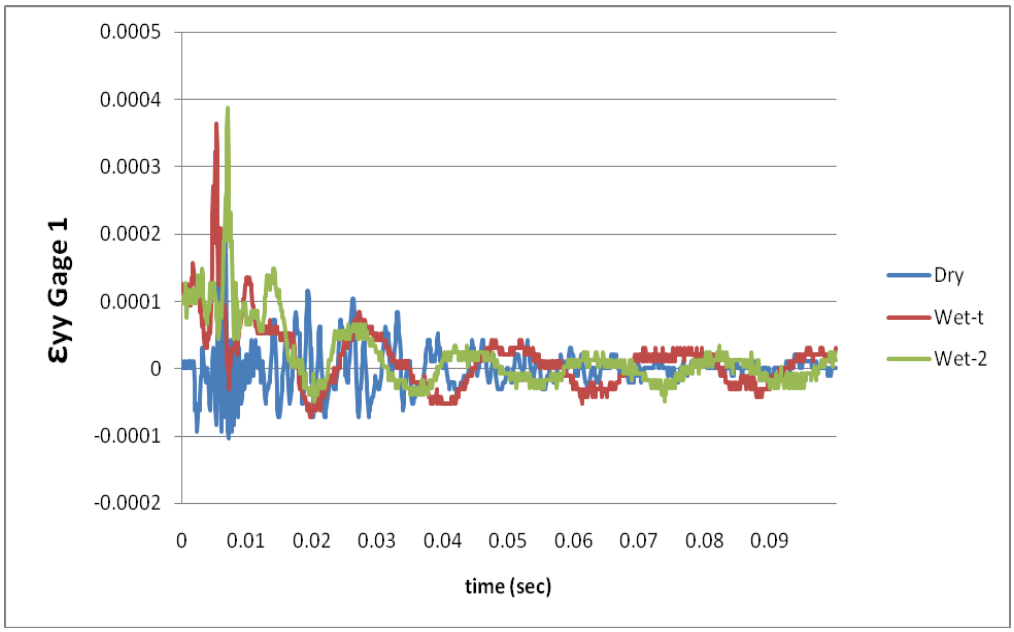

Figure 22. Representative ε_{yy} gage 1 response

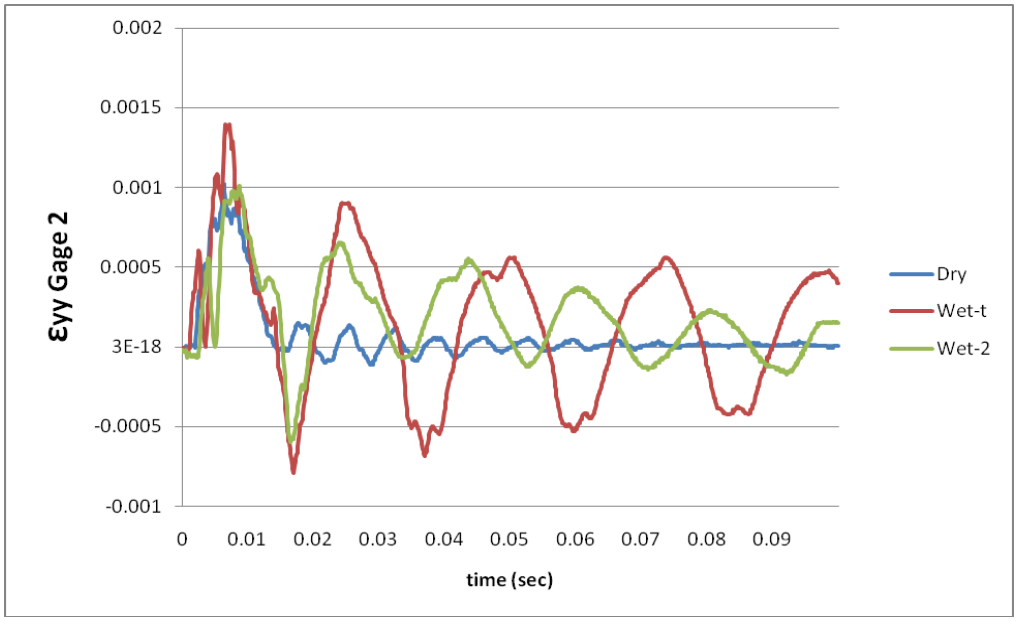

Figure 23. Representative ε_{yy} gage 2 response

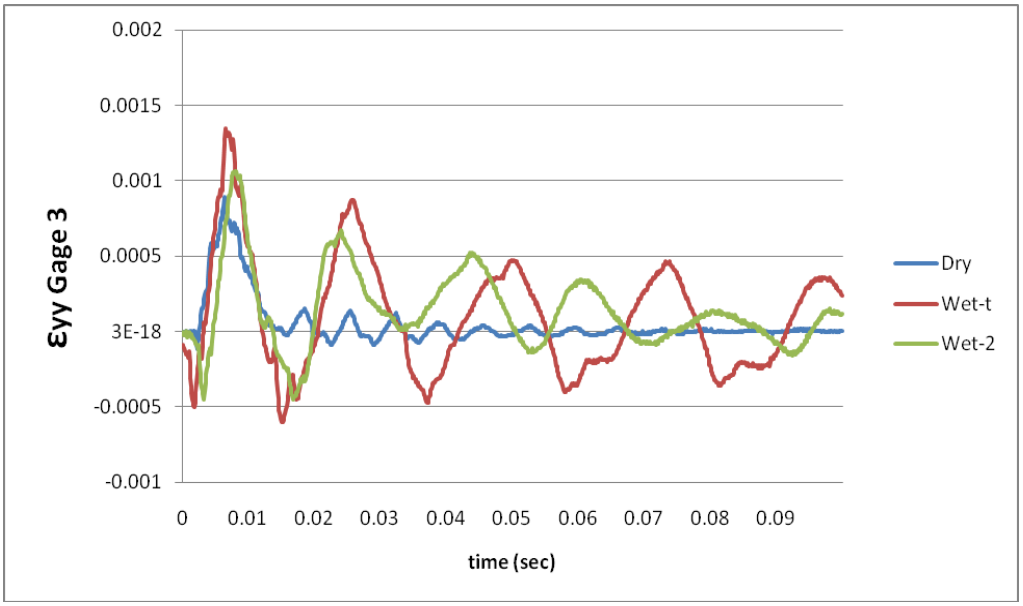

Figure 24. Representative ε_{yy} gage 3 response

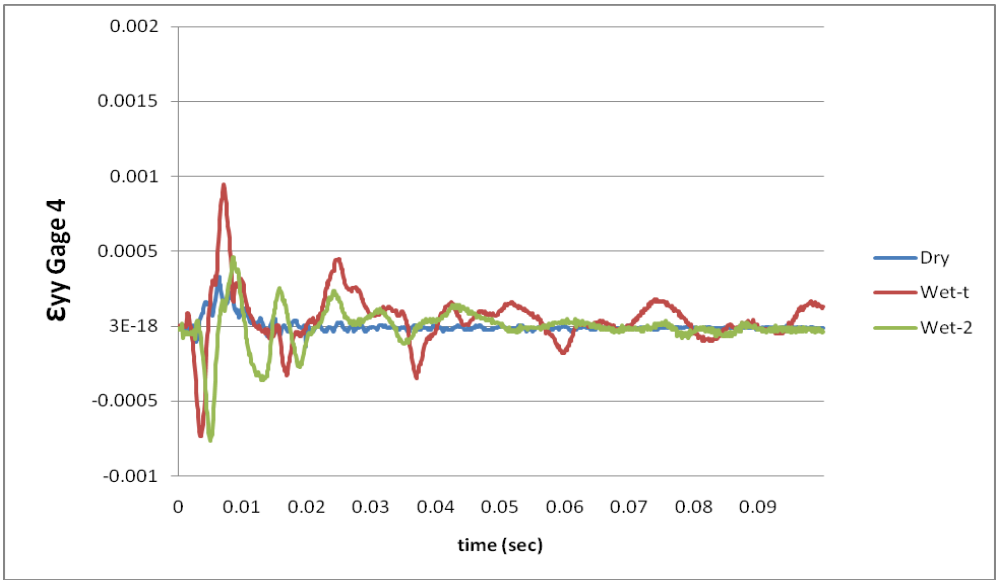

Figure 25. Representative ε_{yy} gage 4 response

Figures 18–25 show the composite structural response to low velocity impact of air-backed and water-backed surroundings as compared to dry. The FSI with either air-backed or water-backed significantly influences both the magnitude and frequency of the strain on the composite.

For gage 1, located directly opposite the impact, Figures 18 and 22, showed the highest magnitude ratio in comparison to the baseline than the other gage locations. The scale for gage 1 plot was adjusted to provide a more easily readable plot. The ratios of peak strains are even higher than the ratio of impact forces. The gage offset was adjusted to a zero baseline, which gives the impression that the strain value is less at gage 1 than the other gages, which intuitively should be the highest value. This result requires further investigation, specifically with regard to the strain rosette response at this location.

As expected, the natural frequencies of both wet cases were lower than the dry case, illustrative of the added mass effect. The frequency for the dry impact case is more than double both of the wet cases. The ratio of peak strains between both wet cases is greater than the ratio of peak impact force. Table 3 lists the experimental values for comparison. Of note, the air-backed wet case had the lowest frequency, which indicates that the lack of fluid on one side of the plate has an influence on the added mass effect.

In previous studies, it was observed that changes in height below the surface of a submerged structure caused changes the added mass effect by increasing the frequency as the structure approached the surface [14]. In this case, the air-backed plate had an even lower frequency than the water-backed case.

As shown in Figure 17, the impact force peak occurs last for the dry case; however, in all gages the peak strains occur almost at the same time.

In all gage locations, both wet cases have higher amplitudes of the initial peak than the dry; yet again, the air-backed case is higher than the water-backed. Gages 3 and 2 have a smaller ratio of dry and wet peak amplitudes. Gage 4 has the greatest peak ratio between the air-backed and the dry case. Of note, the strains for the dry impact show a high initial peak followed by very low magnitudes of oscillation, whereas, both wet cases show a higher initial peak with high magnitudes of subsequent oscillations. The decay of the water-backed case was greater than the air-backed as expected, due to a greater damping effect of water on both sides.

In comparing strains along x-axis versus along y-axis, the magnitudes at each gage are fairly comparable. The small differences are probably due to their location differences along the axis and their orientation.

Strains near the boundary, gage 4 (Figures 21 and 25), and gage 3 (Figures 19 and 23), show a much greater FSI effect—that is, the magnitudes for both wet cases in gage 4 and 3 are much greater than the dry, and have a high initial compressive strain that does not even occur in the dry case. The initial compressive strain is due to the clamped boundary constraint. Following the initial compressive strain, the air-backed wet case has a high tensile strain, whereas the water on both sides of the water-backed case seems to decrease the secondary tensile peak, especially at gage 4. Gage 4 has a higher initial compressive peak than gage 3 because it is closer to the boundary.

2. Experimental Natural Frequency and Damping Ratio Calculations

The strain gage plots were used to determine the damping ratio and the natural frequency for the system. The damped natural frequency was determined by measuring the period of damped oscillations from the strain plot after the initial force response in order to capture the responses of the free vibration of the composite plate [19]. To improve the accuracy, several periods, starting from the first free vibration oscillation peak, were considered using the following equation:

$$T = \frac{t_n - t_l}{n-1}$$

The period was then used to determine the experimental damped natural frequency:

$$\omega_d = \frac{2\pi}{T}$$

The amplitudes x_n and x_l , illustrated in Figure 26, were then used to determine the experimental damping ratio:

$$\zeta = \frac{\frac{1}{n-1}\ln\left(\frac{x_l}{x_n}\right)}{\sqrt{4\pi^2 + \left[\frac{1}{n-1}\ln\left(\frac{x_l}{x_n}\right)\right]^2}}$$

Using the experimental damped natural frequency and damping ratio, the natural frequency was calculated:

$$\omega_n = \frac{\omega_d}{\sqrt{1-\zeta^2}}$$

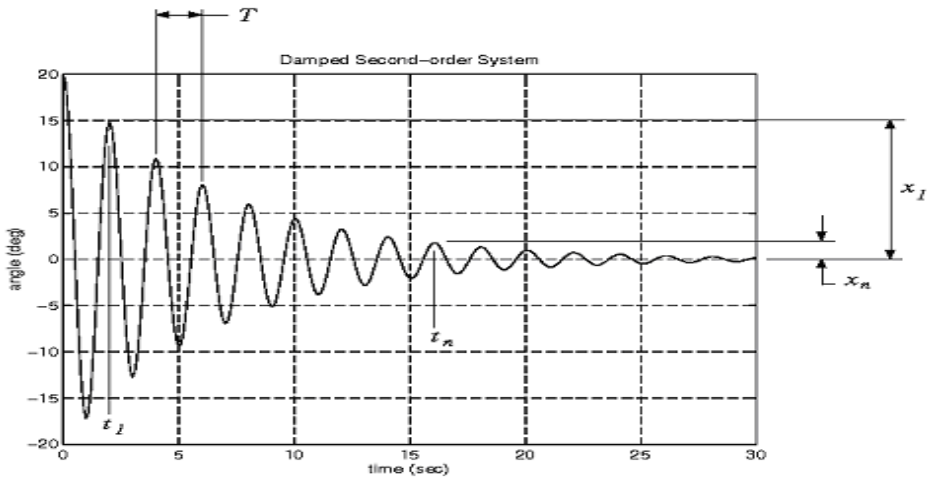

Figure 26. Second order system response calculations

The results for the experimental natural frequency and damping ratio calculations of a representative sample of gage 3 and gage 2 are summarized in Table 3. Gage 4 strain readings were much less harmonic due to the boundary constraint, which made it difficult to get a reliable natural frequency and damping ratio. Also, gage 1, due to its location directly opposite the impact force, did not provide a reliable natural frequency and damping coefficient. Therefore, gages 3 and 2 were used for calculations because of their well defined oscillatory behavior. The full results for each gage are included in Appendix A.

The vibration frequency is the lowest for the air-backed wet impact case, and the highest for the dry impact, also represented in the plots. The frequency for the dry impact case is more than double both of the wet cases. The added mass effect appears to have a greater influence on the air-backed case, but further investigation would be necessary to verify.

The damping ratio for the water-backed case was the highest, as expected due to greater energy dissipation to water on both sides. The average damping ratio of dry, air-backed and water-backed of gages 3 and 2 were 0.053, 0.061, and 0.1055, respectively.

Table 3. Experimental natural frequencies and damping ratios

		T (sec)	ωd (rad/sec)	ζ	ωn (rad/sec)
Dry	ε3x	0.010	645.758	0.0651	647.130
	ε2x	0.010	657.592	0.0824	659.836
	ε3y	0.010	655.875	0.0308	656.186
	ε2y	0.010	655.875	0.0399	656.397
Wet-t	ε3x	0.034	187.463	0.0646	187.856
	ε2x	0.033	189.442	0.0533	189.711
	ε3y	0.033	189.442	0.0735	189.956
	ε2y	0.033	189.157	0.0527	189.419
Wet-2	ε3x	0.026	241.660	0.1442	243.140
	ε2x	0.026	242.471	0.1086	243.914
	ε3y	0.026	242.004	0.1063	243.384
	ε2y	0.025	247.244	0.0614	247.712

3. Added Mass Calculations

Conventionally, experimentally determined natural frequencies of plates immersed in water are compared to that in a vacuum to determine the effective change denoted by calculations of an added virtual mass incremental factor (AVMIF) [16]. The AVMI factor, β, is the ratio of the kinetic energy of water to that of the plate. The AVMI factor is calculated from the approximate formula:

$$\omega_w = \frac{\omega_a}{\sqrt{1+\beta_{mn}}}$$

where ω_w is the natural frequency in water and ω_a is the reference natural frequency. The AVMI factor depends on the mode shape, but it has been proven [16] that at lower modes, the mode shape only changes slightly between vibration in air to that of vibration in water, so that the approximation formula provides very good accuracy for lower modes. The calculated AVMI factors for this study for gages 3 and 4 are summarized in Table 4. These values provide a ratio of the change in frequency due to the added mass effect of the water to the plate vibration. The AVMI factors for all gages are included in

Appendix B. Published AVMI factors for steel submerged in water range from 1.4 to 2.4 depending on the boundary conditions [14, 17], whereas, for this study the average AVMI factor for water-backed case was significantly higher at 6.6. This quantitatively shows the significance of the added mass effect of water on composites which have comparable densities.

Table 4. Experimental added virtual mass incremental factors

		ωn (rad/sec)	Dry ωn (rad/sec)	β factor
Wet-t	**ε3x**	173.3422	615.6221	11.61
	ε2x	176.6594	661.6360	13.03
	ε3y	179.1838	633.4428	11.50
	ε2y	173.2472	614.7481	11.59
Wet-2	**ε3x**	223.4895	615.6221	6.59
	ε2x	238.2935	661.6360	6.71
	ε3y	226.9937	633.4428	6.79
	ε2y	226.8572	614.7481	6.34

C. VELOCITY OF IMPACT COMPARISON

In phase IV testing, the surroundings of the composite held constant and the height varied in order to vary the velocity of impact and investigate the response. There were three heights used, 1.07 m, 0.76 m, and 0.46 m, which corresponds to velocities of 4.6 m/sec, 3.9 m/sec, and 3 m/sec. Each varied height was tested in each environmental surrounding. Figures 27–36 illustrate a representative sample of the dynamic response of the composite plate under wet-t surroundings and wet-2 surroundings compared to the dry baseline representative sample.

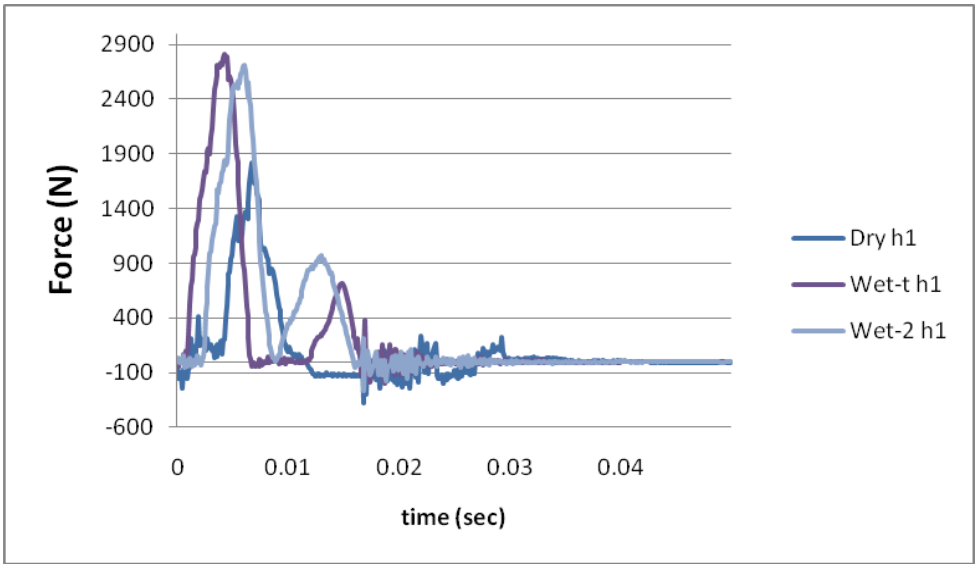

Figure 27. Representative transient force response at 4.6 m/sec velocity

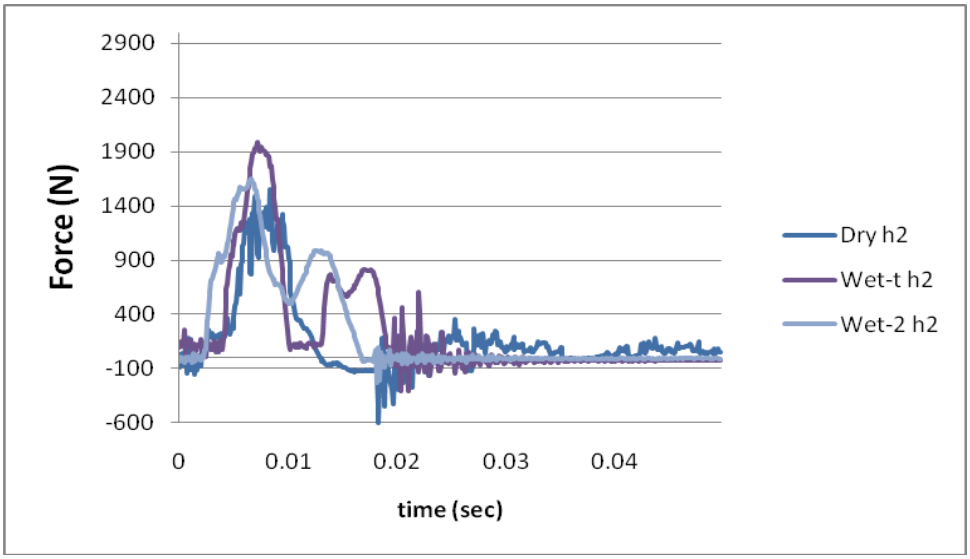

Figure 28. Representative transient force response at 3.9 m/sec velocity

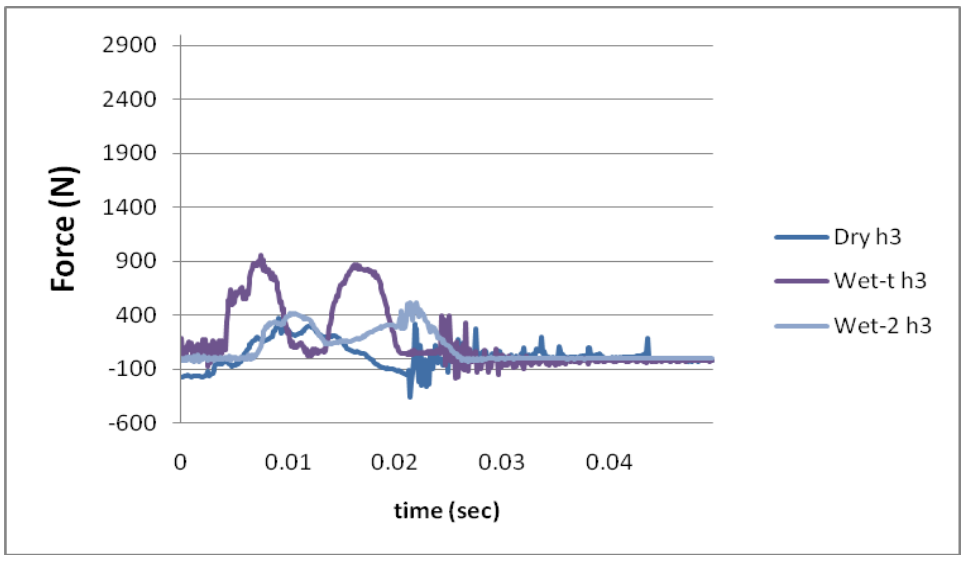

Figure 29. Representative transient force response at 3 m/sec velocity

The peak impact force occurs earliest for both wet case for all three velocities. Both wet cases show a delay and small oscillatory response prior to the initial impact peak in the two lower velocities, which did not occur in the full velocity. The air-backed wet case has the highest magnitude of impact force for all three velocities. Also, the dry case in all three velocities shows more oscillation at the peak, especially at 3.9 m/s, because the damping is less as calculated in the prior section.

The second peak force for both wet cases is a second impact that was not prevented by the spring which does not show in the dry case in all three velocities. The air-backed case displayed a delay between impacts, whereas in the water-backed case the secondary peak immediately followed the initial peak, especially evident in the 3.9 m/s velocity.

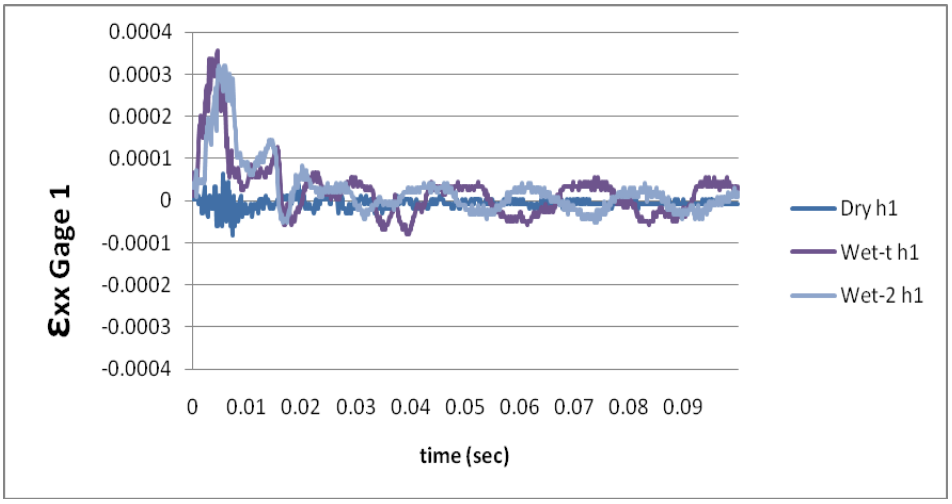

Figure 30. Representative ε_{xx} gage 1 response at 4.6 m/sec velocity

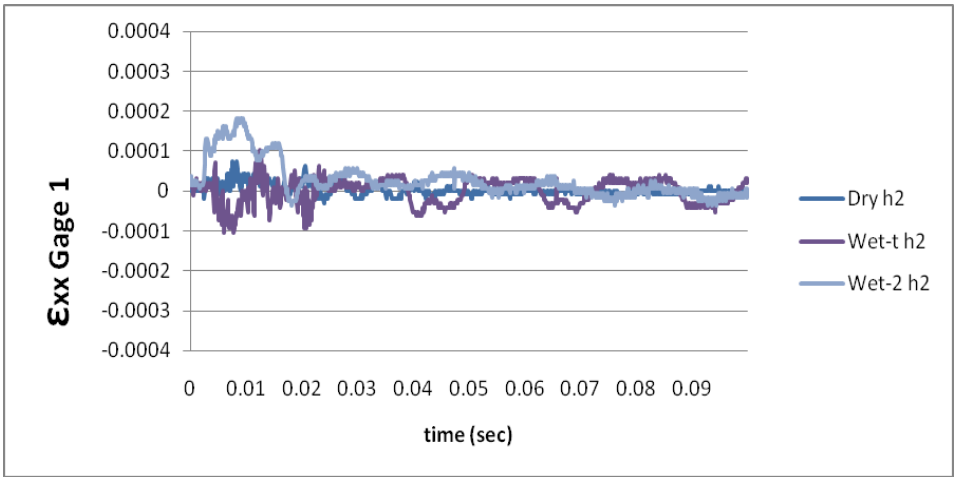

Figure 31. Representative ε_{xx} gage 1 response at 3.9 m/sec velocity

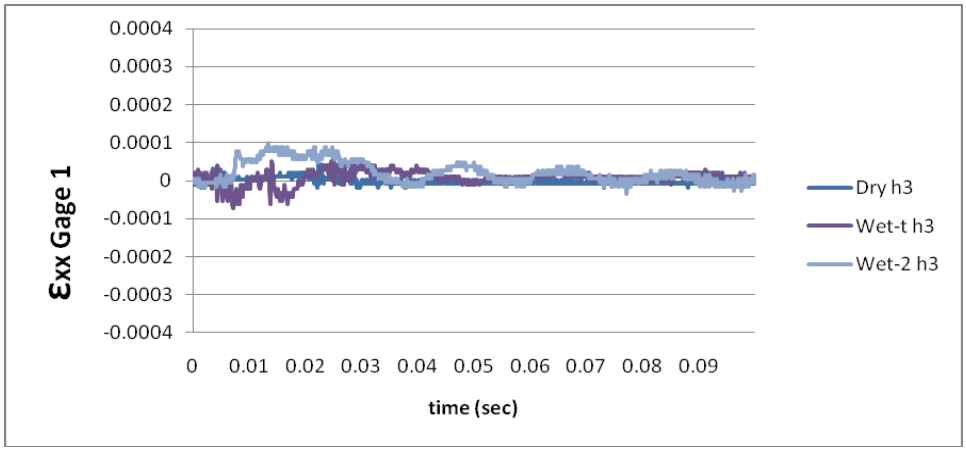

Figure 32. Representative ε_{xx} gage 1 response at 3 m/sec velocity

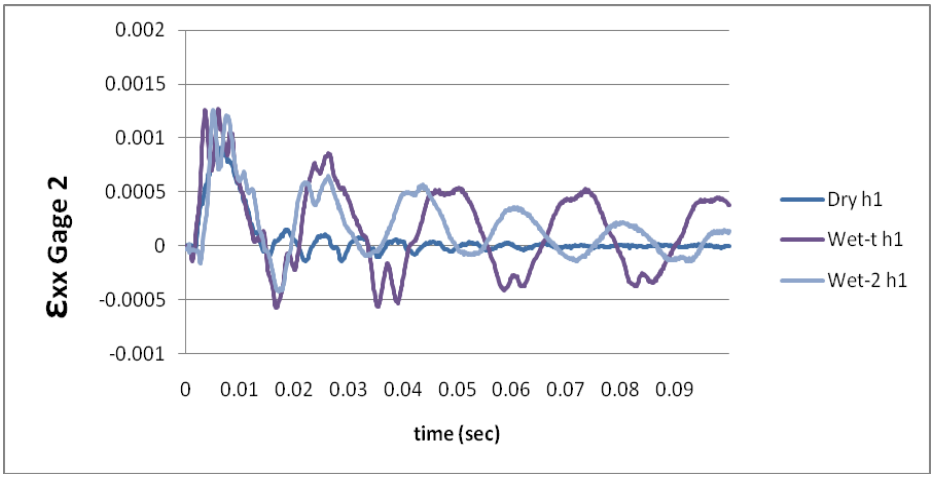

Figure 33. Representative ε_{xx} gage 2 response at 4.6 m/sec velocity

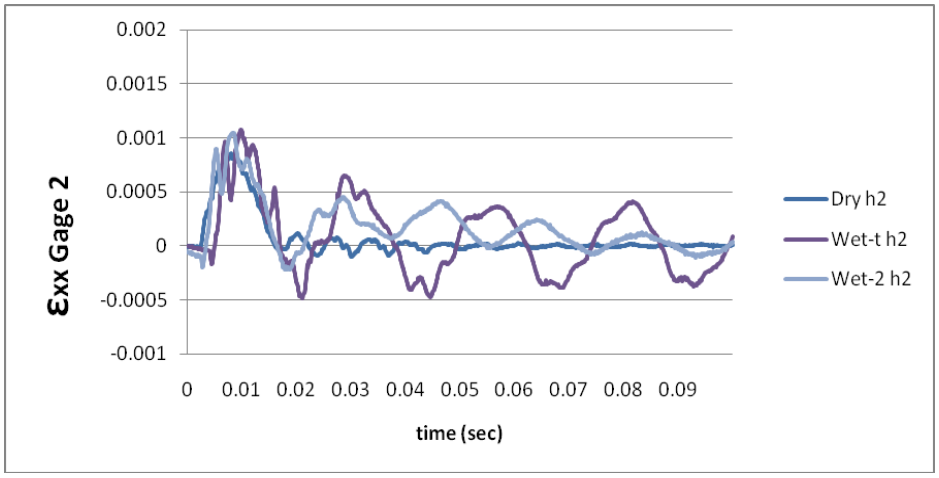

Figure 34. Representative ε_{xx} gage 2 response at 3.9 m/sec velocity

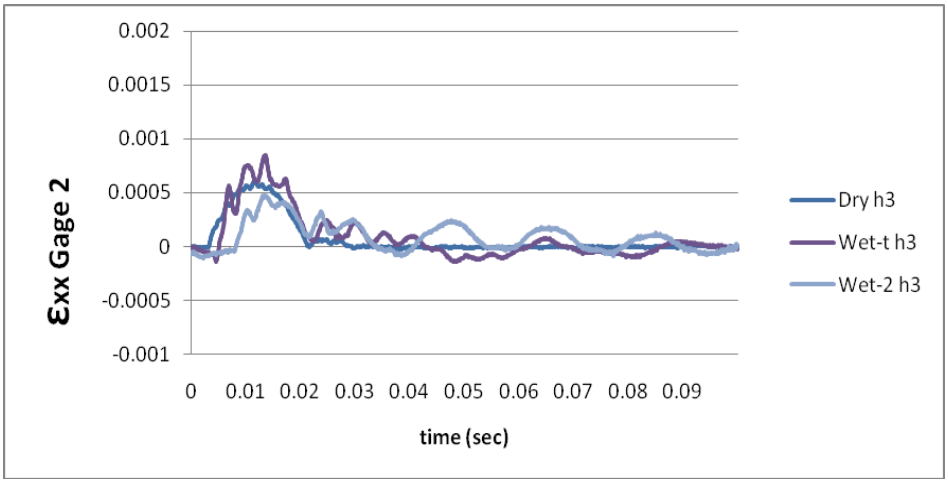

Figure 35. Representative ε_{xx} gage 2 response at 3 m/sec velocity

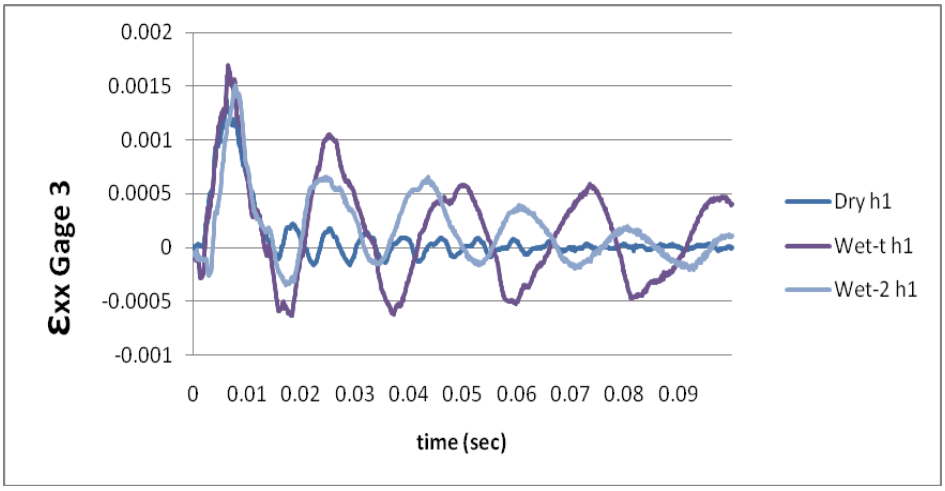

Figure 36. Representative ε_{xx} gage 3 response at 4.6 m/sec velocity

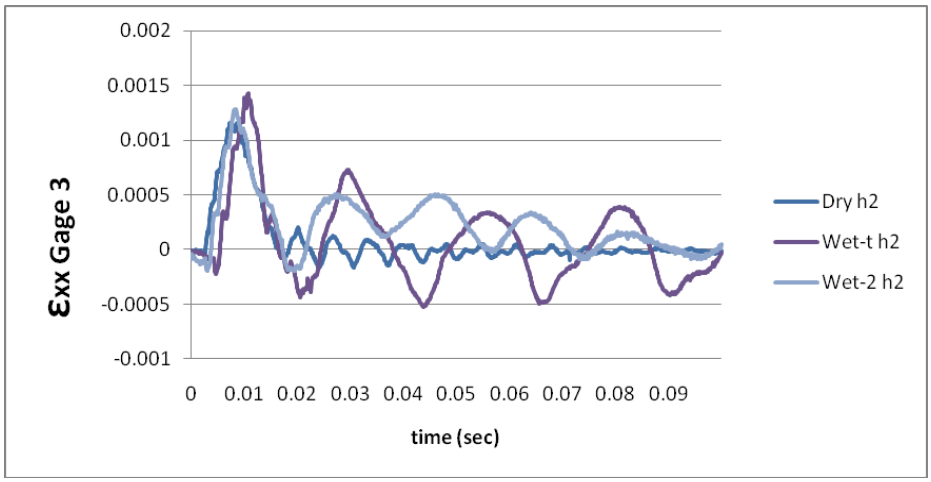

Figure 37. Representative ε_{xx} gage 3 response at 3.9 m/sec velocity

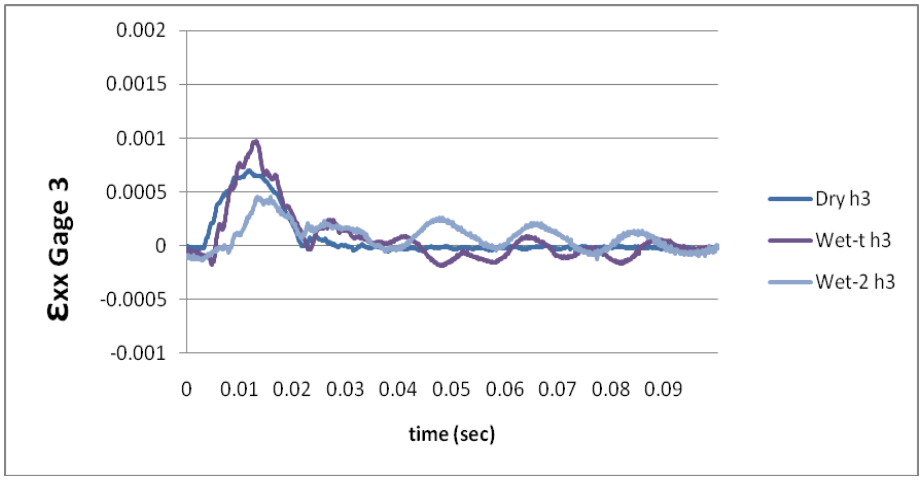

Figure 38. Representative ε_{xx} gage 3 response at 3 m/sec velocity

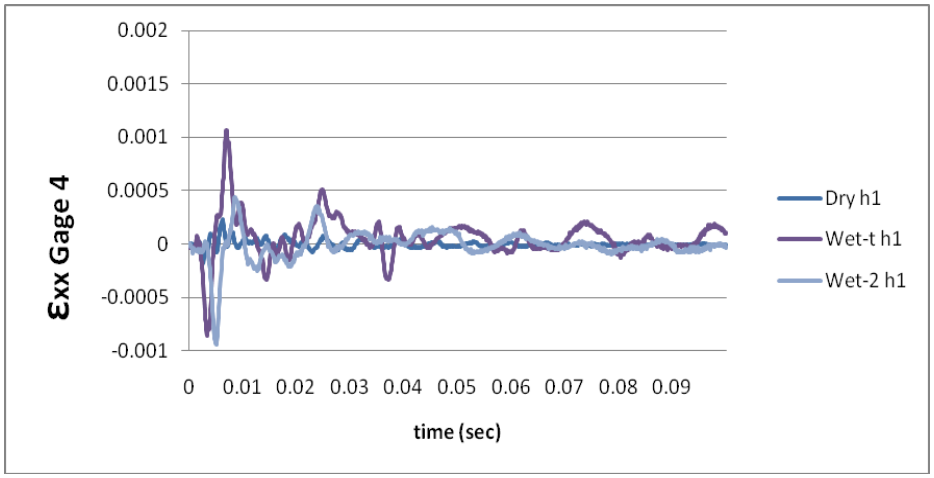

Figure 39. Representative ε_{xx} gage 4 response at 4.6 m/sec velocity

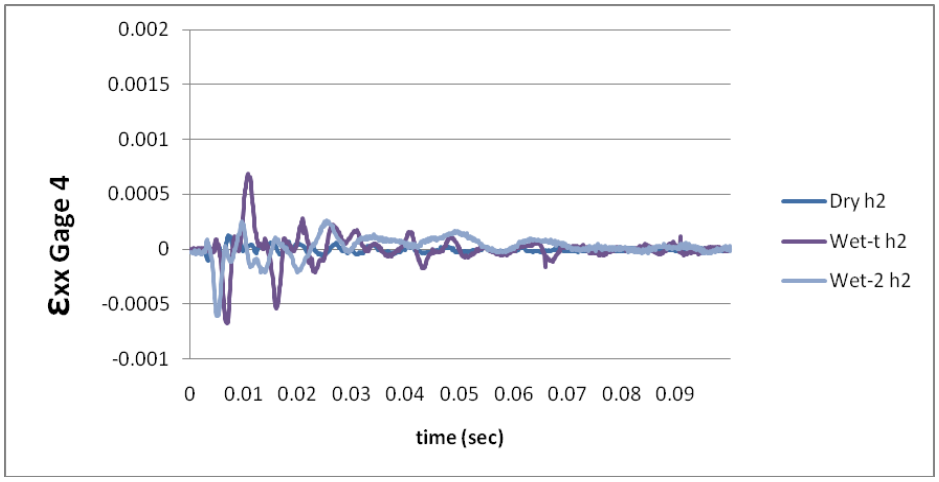

Figure 40. Representative ε_{xx} gage 4 response at 3.9 m/sec velocity

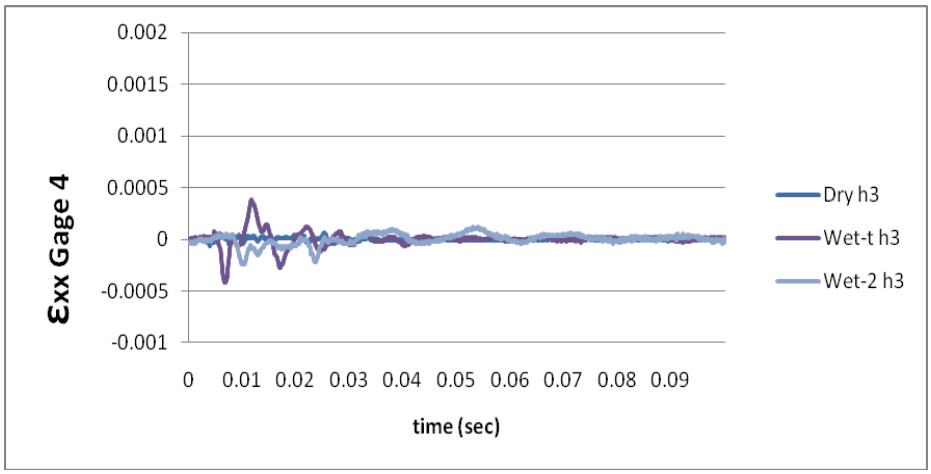

Figure 41. Representative ε_{xx} gage 4 response at 3 m/sec velocity

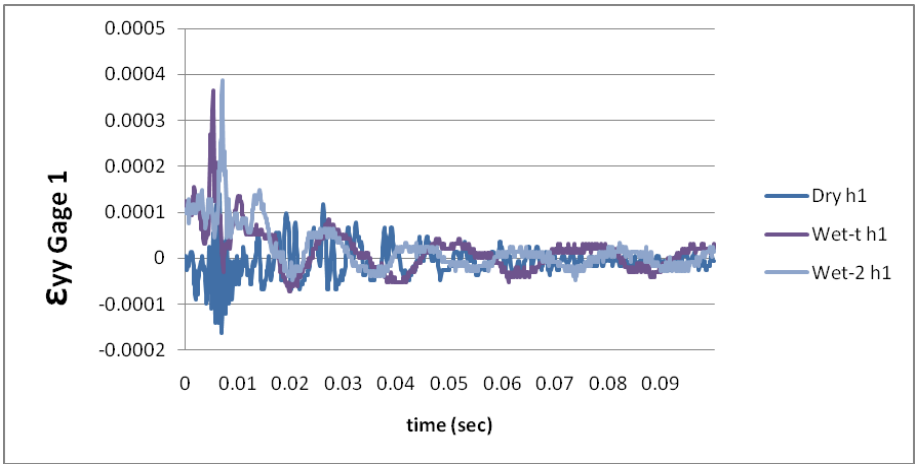

Figure 42. Representative ε_{yy} gage 1 response at 4.6 m/sec velocity

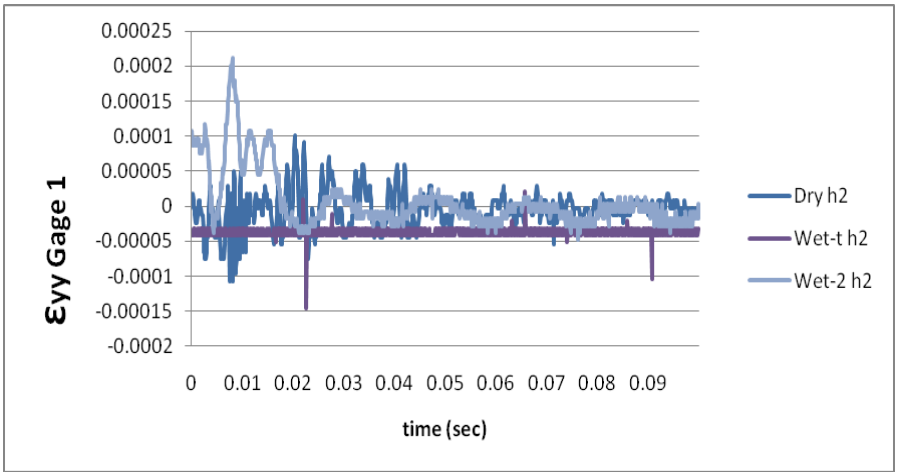

Figure 43. Representative ε_{yy} gage 1 response at 3.9 m/sec velocity

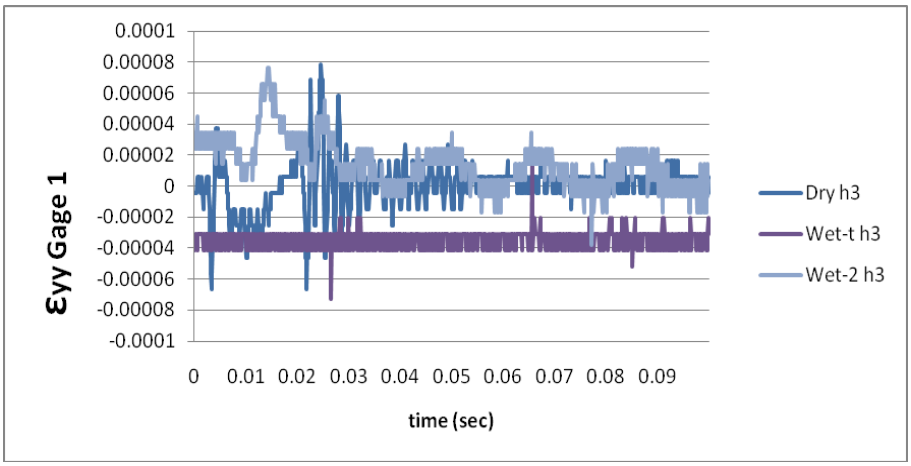

Figure 44. Representative ε_{yy} gage 1 response at 3 m/sec velocity

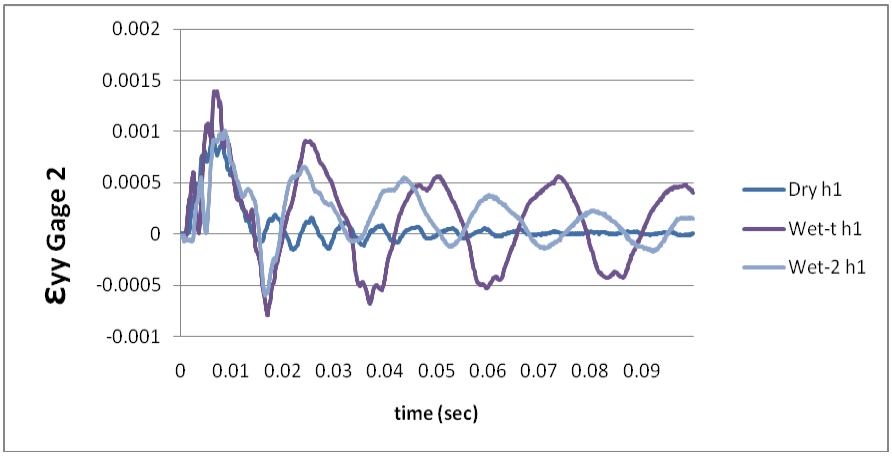

Figure 45. Representative ε_{yy} gage 2 response at 4.6 m/sec velocity

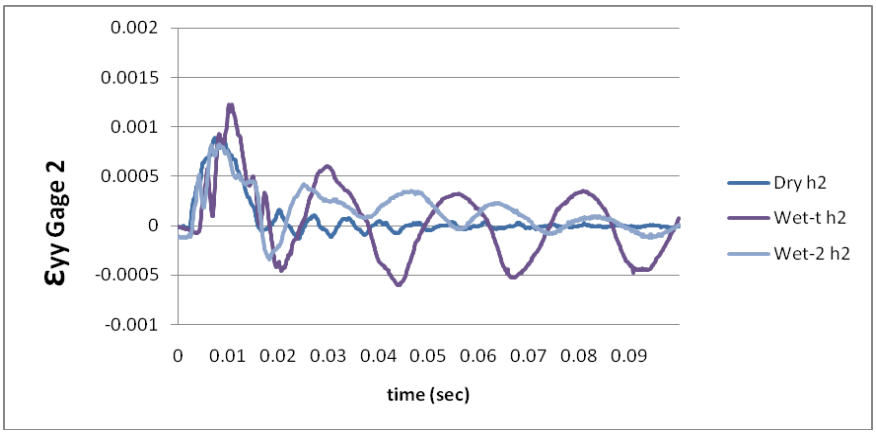

Figure 46. Representative ε_{yy} gage 2 response at 3.9 m/sec velocity

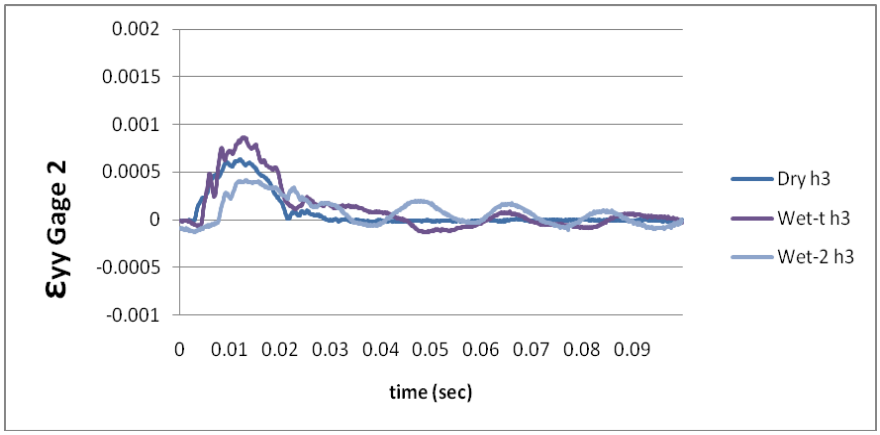

Figure 47. Representative ε_{yy} gage 2 response at 3 m/sec velocity

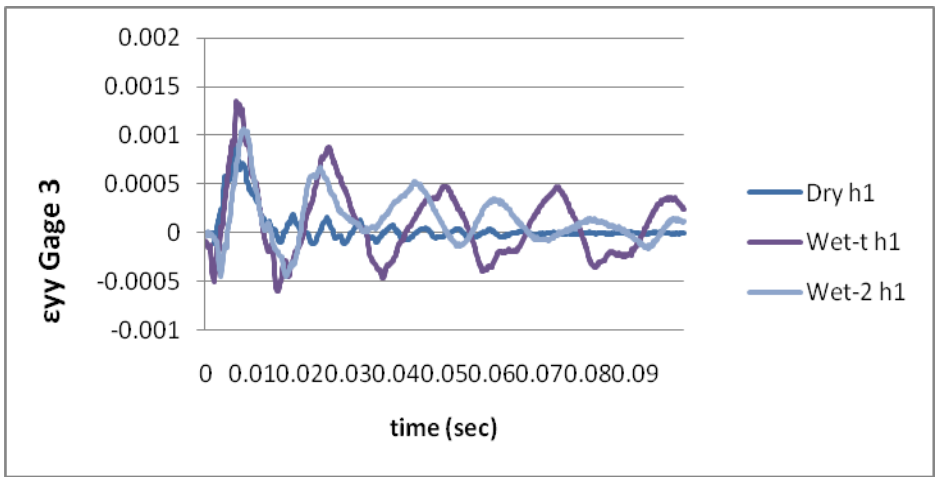

Figure 48. Representative ε_{yy} gage 3 response at 4.6 m/sec velocity

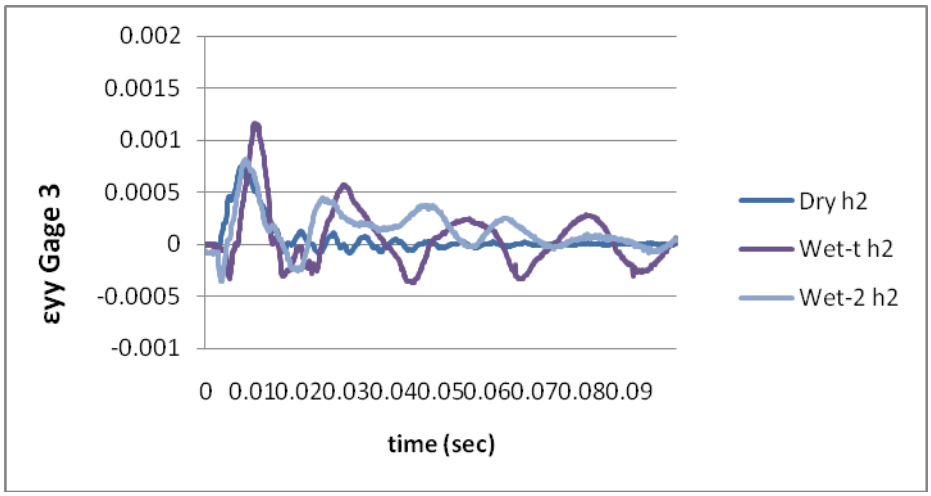

Figure 49. Representative ε_{yy} gage 3 response at 3.9 m/sec velocity

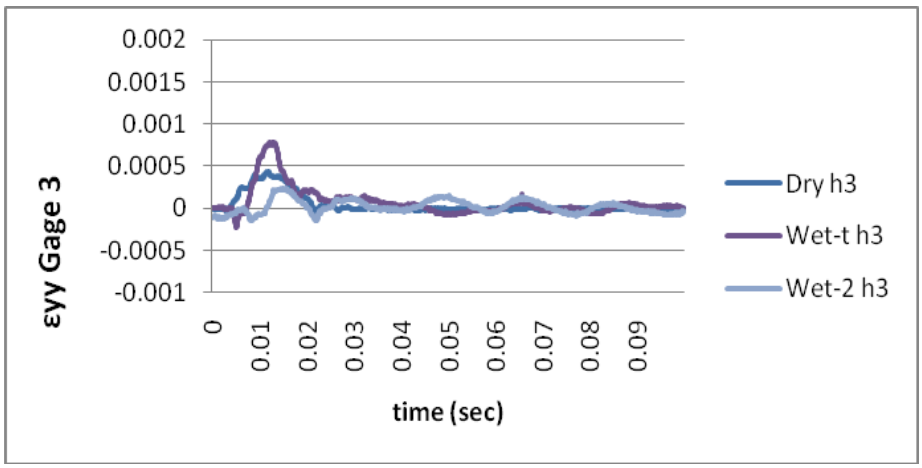

Figure 50. Representative ε_{yy} gage 3 response at 3.9 m/sec velocity

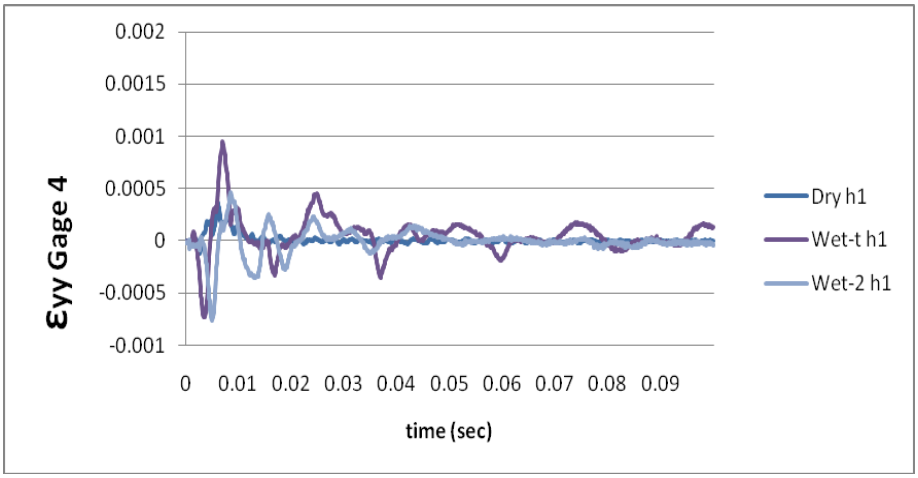

Figure 51. Representative ε_{yy} gage 4 response at 4.6 m/sec velocity

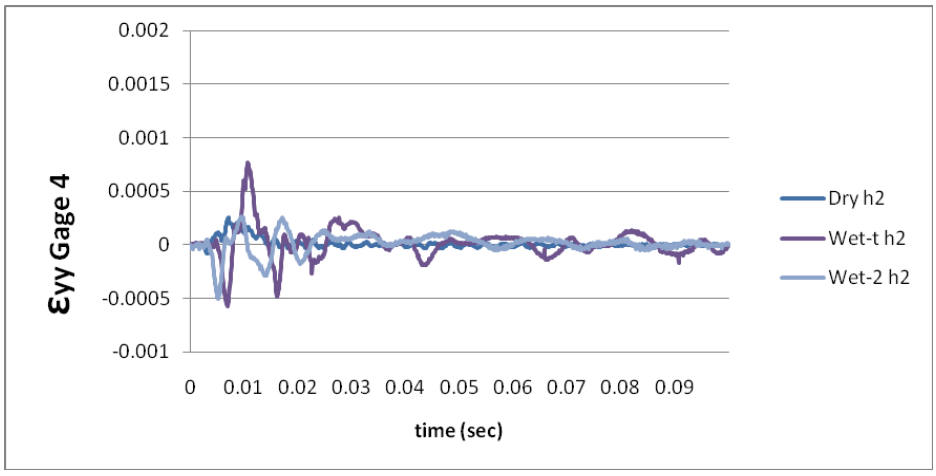

Figure 52. Representative ε_{yy} gage 4 response at 3.9 m/sec velocity

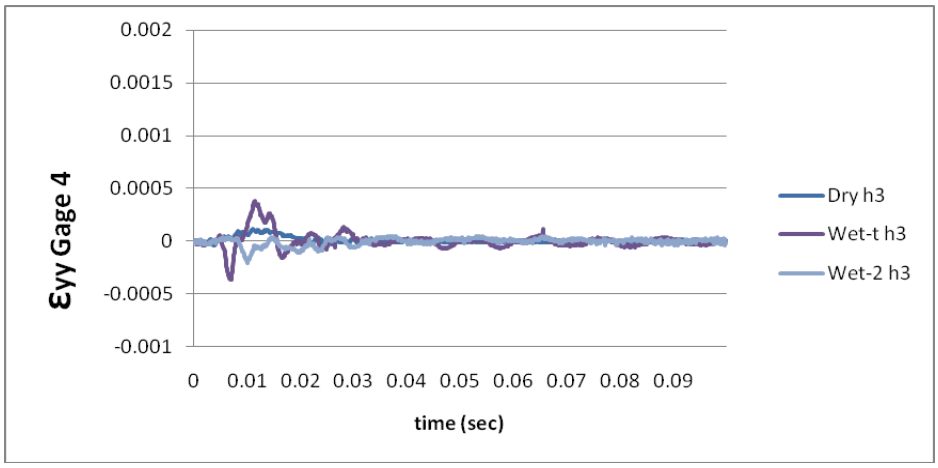

Figure 53. Representative ε_{yy} gage 4 response at 3 m/sec velocity

Figures 30–53 show the composite structural response for varied impact velocities of air-backed and water-backed surroundings as compared to dry. Gage 1 along the y-axis appears to have delaminated in the two lower velocities. The FSI for both air-backed and water-backed significantly influences both the magnitude and frequency of the strain on the composite at all three velocities with some minor differences in the lowest velocity. FSI does not appear to be influenced by the velocity of impact in that there are no clear trends of changes from one velocity to the next. The lowest velocity had the greatest effect on the water-backed case in the magnitude and delay of impact force and subsequently the peak strain.

In all three velocities, the natural frequencies of both wet cases were lower than the dry case, illustrative of the added mass effect. The frequency for the dry impact case is more than double both of the wet cases. Of note, the air-backed wet case had the highest magnitude of initial peak and lowest frequency for all three velocities. The water-backed case had an equally high magnitude as the air-backed in the high and median velocity, but a significantly lower magnitude in the low velocity that coincides with the significantly lower impact force (Figure 29).

In comparing the timing of the initial strain peak, the air-backed case occurs first for 4.6 m/s, last for 3.9 m/s, and in the middle for 3 m/s. The water-backed case had the longest delay to initial strain peak for the lowest velocity which coincides with the longer delay of the impact force (Figure 29).

The strains for the dry impact show a high initial peak followed by very low magnitudes of oscillation, whereas, both wet cases show a higher initial peak with high magnitudes of subsequent oscillations even in the lowest velocity.

In comparing strains along x-axis versus along y-axis, the magnitudes at each gage are fairly comparable, slightly higher along the y-axis. The small differences are probably due to their location differences along the axis and their orientation.

Strains near the boundary, gage 4 and gage 3, show a much greater FSI effect, that is, the magnitudes for both wet cases in gage 4 and 3 are much greater than the dry, and have a high initial compressive strain that does not even occur in the dry case. Gage 4

has the greatest peak ratio between the air-backed and the dry case. The magnitude of the tensile strain of the air-backed case was significantly higher than the water-backed case for all three velocities.

V. CONCLUSIONS AND RECOMMENDATIONS

In this study, a series of experiments was conducted to study the dynamic response of a square composite plate submerged in water subjected to a low velocity impact. The results of this study concluded that the added mass effect of FSI had a significant influence on the magnitude and frequency of the impact force and strain of the composite sample. The magnitude of the strain response varied significantly with location on the plate. On average, the effect of added mass from the high density of water resulted in a 50% greater impact force, a 20%-50% increase in strain, and a decrease of more than half in frequency for composites submerged in water. These results support how much more important FSI is in relatively dense fluids such as water. The AVMI factors for this study, which is the ratio of the kinetic energy of water to that of the plate, were on average 11.95 for the air-backed case and 6.6 for the water-backed case. Results from this study also indicated that FSI does not appear to have a proportional influence by the velocity of impact.

A tremendous amount of effort has been given to develop methods to predict the magnitude of the added mass effect of vibrating structures submerged in fluid. This experimental study will hopefully initiate that effort into investigations of the added mass effect on composite structures due to their increase in use in naval architecture.

Future studies should include, but not limited to, further investigation on the dynamic response of air-backed samples, developing analytical methods for predicting added mass effect on composites, and investigating types of damage and damage thresholds for composites submerged in or in contact with water and subjected to low velocity impact.

APPENDIX A: EXPERIMENTAL NATURAL FREQUENCY CALCULATIONS

		T (sec)	ωd (rad/sec)	ζ	ωn (rad/sec)
Dry	**ε1x**	0.009	662.797	0.099366	666.093
Dry	**ε3x**	0.010	645.758	0.065084	647.130
Dry	**ε2x**	0.010	657.592	0.082414	659.836
Dry	**ε4x**	0.008	758.912	0.056824	760.141
Dry	**ε1y**	0.010	640.816	0.01577	640.896
Dry	**ε3y**	0.010	655.875	0.03078	656.186
Dry	**ε2y**	0.010	655.875	0.0399	656.397
Dry	**ε4y**	0.005	1147.032	0.055039	1148.773
Wet-t	**ε1x**	0.033	189.157	0.016367	189.182
Wet-t	**ε3x**	0.034	187.463	0.064646	187.856
Wet-t	**ε2x**	0.033	189.442	0.053279	189.711
Wet-t	**ε4x**	0.033	192.049	0.074118	192.579
Wet-t	**ε1y**	0.034	183.626	0.076462	184.165
Wet-t	**ε3y**	0.033	189.442	0.073542	189.956
Wet-t	**ε2y**	0.033	189.157	0.052654	189.419
Wet-t	**ε4y**	0.033	189.728	0.086648	190.444
Wet-2	**ε1x**	0.028	227.536	0.023517	227.599
Wet-2	**ε3x**	0.026	241.660	0.144241	243.140
Wet-2	**ε2x**	0.026	242.471	0.108628	243.914
Wet-2	**ε4x**	0.026	244.358	0.094648	245.460
Wet-2	**ε1y**	0.028	227.125	0.078996	227.837
Wet-2	**ε3y**	0.026	242.004	0.106328	243.384
Wet-2	**ε2y**	0.025	247.244	0.061444	247.712
Wet-2	**ε4y**	0.017	373.810	0.203266	381.780

APPENDIX B: EXPERIMENTAL AVMI CALCULATIONS

		ωn (rad/sec)	Dry ωn (rad/sec)	β factor
Wet-t	**ε1x**	189.1819678	666.0933754	11.40
	ε3x	187.8556367	647.1304213	10.87
	ε2x	189.7113862	659.8362733	11.10
	ε4x	192.5786259	760.1406107	14.58
	ε1y	184.1648804	640.8960264	11.11
	ε3y	189.9563024	656.1855849	10.93
	ε2y	189.4193818	656.3973706	11.01
	ε4y	190.4443602	1148.773246	35.39
Wet-2	**ε1x**	227.5991768	666.0933754	7.57
	ε3x	243.14	647.1304213	6.08
	ε2x	243.9144078	659.8362733	6.32
	ε4x	245.4598908	760.1406107	8.59
	ε1y	227.8367766	640.8960264	6.91
	ε3y	243.3835636	656.1855849	6.27
	ε2y	247.7121333	656.3973706	6.02
	ε4y	381.7797387	1148.773246	8.05

THIS PAGE INTENTIONALLY LEFT BLANK

LIST OF REFERENCES

[1] A. P. Mouritz, E. Gellert, P. Burchill, K. Challis, Review of Advanced Composite Structures for Naval Ships and Submarines, *Composite Structures* 53 (2001) 21-41.

[2] Z. Aslan, R. Karakuzu, B. Okutan, "The Response of Laminated Composite Plates Under Low-Velocity Impact Loading," *Composites Structures* 59 (2003) 119–127.

[3] S. Abrate, "Impact on Laminated Composites; Recent Advances, " *Applied Mechanics Reviews* 47 (11) (1994) 517-544.

[4] L. H. Strait, M.L. Karasek, and M. F. Amateau, "Effects of Stacking Sequence on the Impact Resistance of Carbon Fiber Reinforced Thermoplastic Toughened Epoxy Laminates," *Journal of Composite Materials*, vol. 26, no. 12, 1992, pp. 1725-1740.

[5] M. V. Hosur, K. Jain, F. Chowdhury, S. Jeelani, M. R. Bhat, and C. R. L. Murthy, "Low Velocity Impact Response of Carbon/epoxy Laminates Subjected to Cold-dry and Cold-moist conditioning," *Composite Structures*, vol. 79, pp. 300-311, 2007.

[6] M. O. W. Richardson and M. J. Wisheart, "Review of Low-Velocity Impact Properties of Composite Materials," *Composite Part A*, vol. 27A, pp. 1123-1131, 1996.

[7] M. V. Hosur, M. R. Karim, and S. Jeelani, "Experimental Investigations on the Response of Stitched/Unstitched Woven S2-glass/SC15 Epoxy Composites Under Single Repeated Low Velocity Impact Loading," *Composite Structures*, vol. 62, pp. 89-102, 2003.

[8] S. Abrate, *Impact on Composite Structures*, Cambridge University Press, Cambridge, 1998.

[9] Sjoblom, P. O., Hartness, J. T., and Cordell, T. M., "On Low-Velocity Impact Testing of Composite Materials," *Journal of Composite Materials*, vol. 22, no. 30, pp. 30-51, 1988.

[10] H. Lamb, "On the vibrations of an elastic plate in contact with water," *Proceeding of the Royal Society (London)*, A 98, pp. 205–216, 1921.

[11] J. H. Powell and J. H. T. Roberts, "On the frequency of vibration of circular diaphragms," *Proceeding of the Royal Society (London)* 35, pp. 170–182, 1923.

[12] U. S. Lindholm, D. D. Kana, W. H. Chu, et al., "Elastic vibration characteristics of cantilever plates in water," *Journal Ship Research*, vol 9, no. 1, pp. 11–22, 1965.

[13] G. C. Volcy, P. Morel, M. Bureau, et al, "Some studies and research related to the hydro-elasticity of steel work," *Proceedings of the 122nd Euromech Colloquium on numerical analysis of the dynamics of ship structures,* pp. 403-406, 1979.

[14] Y. Fu, W. G. Price, "Interactions between a partially or totally immersed vibrating cantilever plate and the surrounding fluid," *Journal of Sound and Vibration,* vol 118, no.13, pp. 495–513, 1987.

[15] M. K. Kwak, K. C. Kim, "Axisymmetric vibration of circular plates in contact with fluid," *Journal of Sound and Vibration,* vol 146, pp 381–389, 1991.

[16] M. K. Kwak, "Hydroelastic vibration of rectangular plates," *Journal of Applied Mechanics,* vol 63, pp 110–115, 1996.

[17] M. R. Haddara and S. Cao, "A study of the dynamic response of submerged rectangular flat plates," *Marine Structures,* vol 9, pp. 913–933, 1996.

[18] J. M. Gere and B. J. Goodno, *Mechanics of Materials*, ed. 7, Cengage Learning, Toronto, ON, 2009, pp. 592-596.

[19] R. S. Figliola and D. E. Beasley, *Theory and Design for Mechanical Measurements*, ed.4, John Wiley and Sons, 2006, pp. 425-446.

INITIAL DISTRIBUTION LIST

1. Defense Technical Information Center
   Ft. Belvoir, Virginia

2. Dudley Knox Library
   Naval Postgraduate School
   Monterey, California

3. Professor Young Kwon
   Naval Postgraduate School
   Monterey, California

4. Research Assistant Professor Jarema M. Didoszak
   Naval Postgraduate School
   Monterey, California

5. Douglas C. Loup
   Naval Surface Warfare Center, Carderock Division
   West Bethesda, Maryland

6. Erik A. Rasmussen
   Naval Surface Warfare Center Carderock Division
   West Bethesda, Maryland

7. Scott W. Bartlett
   Naval Surface Warfare Center Carderock Division
   West Bethesda, Maryland

8. Engineering and Technology Circular Office, Code 34
   Naval Postgraduate School
   Monterey, California

9. Angela C. Owens
   Naval Postgraduate School
   Monterey, California